Helfrich cylinders – instabilities, bifurcations and amplitude equations

Alexander Meiners, Hannes Uecker

Institut für Mathematik, Universität Oldenburg, D26111 Oldenburg, alexander.meiners@uni-oldenburg.de,
hannes.uecker@uni-oldenburg.de

February 28, 2025

Abstract

Combining local bifurcation analysis with numerical continuation and bifurcation methods we study bifurcations from cylindrical vesicles described by the Helfrich equation with volume and area constraints, with a prescribed periodicity along the cylindrical axis. The bifurcating solutions are in two main classes, axisymmetric (pearling), and non–axisymmetric (coiling, buckling, and wrinkling), and depending on the spontaneous curvature and the prescribed periodicity along the cylinder axis we obtain different stabilities of the bifurcating branches, and different secondary bifurcations.

Contents

1 Introduction

The (dimensionless) Canham–Helfrich model [Can70, Hel73] (or spontaneous curvature model) for vesicles with lipid bilayer membranes is based on the energy

$$E(X) = \int_X (H - c_0)^2 \, \mathrm{d}S, \tag{1}$$

where X is a (possibly time t dependent) 2D manifold embedded in $\mathbb{R}^3$ with mean curvature H, and where the parameter $c_0 \in \mathbb{R}$ models an energetically favorable spontaneous (or preferred) curvature. Roughly speaking, the aim is to minimize E for prescribed area $\mathcal{A}(X) = \int_X 1 \, \mathrm{d}S$ and enclosed volume $\mathcal{V}(X)$ (see (68)), i.e., under the constraints

$$q_1(X) := \mathcal{A}(X) - \mathcal{A}_0 = 0 \text{ and } q_2(X) := \mathcal{V}(X) - \mathcal{V}_0 = 0. \tag{2}$$

There are numerous works on this, for instance using the minimization of E to explain the shape of red blood cells, see, e.g., [SZ89, SBL90, Pet83, SL95, Sei97].[1] The minimization proceeds by introducing the Lagrangian

$$F(X, \Lambda) = E(X) + \lambda_1(\mathcal{A}(X) - \mathcal{A}_0) + \lambda_2(\mathcal{V}(X) - \mathcal{V}_0), \tag{3}$$

with Lagrange multipliers $\Lambda = (\lambda_1, \lambda_2)$ (see also Remark 1.2a)), which yields the Euler-Lagrange equation

$$G(X, \Lambda) := \Delta H + 2H(H^2 - K) + 2c_0 K - 2(c_0^2 + \lambda_1)H - \lambda_2 = 0, \tag{4}$$

under variations in normal direction together with the constraints (2), where K is the Gaussian curvature, and Δ the Laplace–Beltrami operator on X. Many works also use (1) to study instabilities of tubular vesicles, e.g., [ZcH89, BZM94, FTGB+99, TSA+01], in particular the so–called pearling and coiling instabilities, see Fig.1(a,b), and Remark 1.2b) for a review of the (physics) literature.

In, e.g., [NY12, RSS24], the constrained L^2–gradient flow associated to (1) is studied, which can be written as

$$\begin{pmatrix} V_t(t) \\ 0 \end{pmatrix} = \begin{pmatrix} G(X(t), \Lambda(t)) \\ q(X(t)) \end{pmatrix}, \tag{5}$$

where $q = (q_1, q_2)$ and $V_t(t)$ is the normal velocity of X, and with now time dependent Lagrange multipliers $\Lambda(t)$ which are determined from (2), such that

$$\frac{\mathrm{d}}{\mathrm{d}t} E(X(t), \Lambda(t)) = -\|V(t)\|_{L^2(X(t))}^2, \quad \frac{\mathrm{d}}{\mathrm{d}t} \mathcal{A}(X(t)) = 0, \quad \text{and } \frac{\mathrm{d}}{\mathrm{d}t} \mathcal{V}(X(t)) = 0, \tag{6}$$

as long as the flow exists. We also refer to [Gar13] and [BDGP23] for introductions to, reviews of, and extended bibliographies concerning geometric flows, both analytically and numerically, and also including mean–field approaches.

A cylinder $\mathcal{C}(r)$ of radius r is a solution to (4) iff

$$\lambda_1 = \frac{1}{2} \left(\frac{1}{2r^2} - 2r\lambda_2 - 2c_0^2 \right). \tag{7}$$

However, $E, \mathcal{A}$ and $\mathcal{V}$ are not well defined for an infinite cylinder, and in the following we restrict to cylinders $\mathcal{C}_L(r)$ of lengths L. For these we have the scaling $E(\mathcal{C}_L(\alpha r); c_0) = E(\mathcal{C}_{\alpha L}(r); c_0/\alpha)$ and

---

[1]For $c_0 = 0$, E is also called Willmore energy. More generally, a term $b \int_X K \, \mathrm{d}S$ can be added to E, where the parameter $b \geq 0$ is called saddle–splay modulus, but due to the Gauss–Bonnet theorem $\int K dS$ is a topological invariant for closed X, and hence can be dropped from the minimization of E, and the same holds for the cylindrical topology considered here.
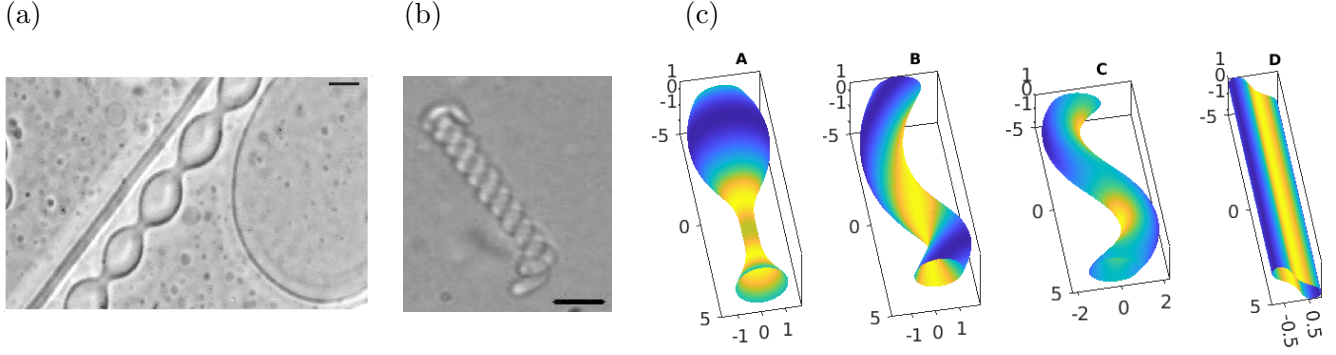
Figure 1: (a,b) Cylindrical vesicle shapes in experiments, pearling (a) from [CR98], and coiling (b) from [HEJ+14]; scale bars representing 10μm. (c) Four types of steady states bifurcating from straight cylinders in (5), with fixed length $L = 10$ (and $c_0 = 0$): A pearling, B coiling, C buckling, D wrinkling; see §5 for detailed bifurcation diagrams and stability information.

thus it is sufficient to consider $r = 1$ with a variable length L, and we abbreviate $\mathcal{C}_L = \mathcal{C}_L(1)$. After showing well–posedness of (5) for initial conditions X_0 close to $\mathcal{C}_L$, where we assume periodic boundary conditions along the cylindrical axis, we study bifurcation diagrams of steady states of (5). In Fig.1(c) we preview four types of solutions from primary branches bifurcating from cylinders, obtained from numerical continuation and bifurcation, namely again pearling (A) and coiling (B) like in (a) and (b), and buckling (C), and wrinkling (D).[2]

The starting point for the bifurcation analysis is the dispersion relation $\mu = \mu(m, n)$ for the linearization of (5) at $\mathcal{C}_L$, which can be computed explicitly from an ansatz $X = C_1 + e^{\mu t + i(k_m x + n\vartheta)} N$, $m, n \in \mathbb{N}$, $k_m = 2\pi m/L$, and where x is along the cylindrical axis and ϑ the polar angle orthogonal to it. We study these dispersion relations with c_0 and λ_2 (and λ_1 given by (7)) as primary parameters, and given c_0 (and L) we typically find narrow ranges in λ_2 of stability of the "trivial branch" $X = \mathcal{C}_L$, with branch points at the ends. At one end, axisymmetric branches of pearling type A bifurcate, while at the other end the loss of stability may be with respect to any of B,C or D.

After identifying these instabilities, based on the well–posedness results for the flow we use a centre manifold reduction to derive amplitude equations (AEs) for the critical modes, and from these also obtain approximations of the bifurcating steady state branches. The derivation of these AEs is rather non–standard due to the constraints (2), and in some sense our methods could be described as bifurcation without parameters [Lie15], see Remark 1.1.

Finally, we use the package `pde2path` [Uec21, MU24b] to numerically continue the primary bifurcating branches away from their bifurcation points from $\mathcal{C}_L$. Close to bifurcation these numerical results agree well with the AE description, and additionally we obtain the behavior and stability at larger amplitude, and secondary bifurcations. In summary, this yields rather complicated bifurcation diagrams (BDs), which we discuss in detail for three exemplary cases, namely $c_0 = 0, c_0 = -1$, and $c_0 = 0.48$, with strong qualitative differences, and we complement these steady state BDs with numerical flows for (5) to give further indication of the typical behavior of (5).

Remark 1.1. We start the linear stability analysis and also the numerical bifurcation analysis by continuation of the trivial solution (branch) $\mathcal{C}_L$ in the Lagrange multiplier λ_2 (with λ_1 given by (7)). We then also often continue the nontrivial branches (e.g., of type A–D from Fig.1) in λ_2 as a primary parameter, with fixed $\mathcal{A}$ but without fixing $\mathcal{V}$. However, the stability is always computed wrt to (5), i.e., for the area and volume conserving flow. This point of view of allowing the volume $\mathcal{V}$ to change along the branch while considering stability under $\mathcal{V}$ conservation is motivated by the closed vesicle

---

[2]While pearling is a standard name for A, the nomenclature for B and in particular C varies. For instance, B is sometimes called writhing or twisting, and in [NSS15], C is called wrinkling. We could not find explicit names for states like D in the "vesicles literature", and our choice of "winkling" is inspired by [FVKG22], which treats a related model for arteries with a restoring force.

situation discussed for example in [JSL93] and [MU24b]. Roughly speaking, the sphere is the unique maximum of volume at fixed area, and hence volume and area preserving branches bifurcating from the sphere do not exist. The same holds for the cylinder if we also fix the length L. Cylinders can be destabilized preserving $\mathcal{V}$ and $\mathcal{A}$ when allowing L to change, see, e.g., [ZcH89], but we found our method with fixed L more convenient. ⌋

Remark 1.2. a) The spontaneous curvature parameter c_0 depends on the properties of the lipid bilayer membrane and can be positive or negative. λ_2 is the pressure difference between inside and outside; since we choose the inner normal, here negative λ_2 corresponds to lower pressure inside. λ_1 corresponds to a surface tension, and can also have either sign; see, e.g., [BHAVMC17] for discussion.

b) Following [BZM94], [GNPS96] considers the dynamics of pearling based on the Helfrich energy and treating the hydrodynamics in the tube via a lubrication approximation. This leads to a 6th order Cahn–Hilliard type equation for axially symmetric perturbations of the cylinder, with $\mathcal{V}$ conservation, and the critical wave numbers and growth rates of the pearling (including the propagation speed of pearling fronts) are carefully compared to [BZM94]. The coiling instability and the dynamics of coiling are discussed [FTGB+99, TGBKS01], and compared to the dynamics of pearling in [TSA+01]. For both, it is argued that polymers anchoring at lipid bilayers *locally* generate nonzero values for the spontaneous curvature c_0, *and* generate significant differences in effective area between inside and outside of the bilayer(s), which points at area difference elasticity (ADE) terms. In particular, in [TSA+01], measurements of diffusion/propagation speeds suggest that for local injection of polymers in the outer fluid, initially ADE terms (with bulk diffusion of polymers) give the right model, and SC terms (with surface diffusion of polymers) when reaching equilibrium, both with $\mathcal{A}$ and $\mathcal{V}$ conservation. On the other hand, [CR98] argues that in certain experiments $c_0 \neq 0$ is a global quantity. Finally, an important feature of coiling is that it rather occurs for multilamellar tubes, and that in equilibrium the coiling is usually "tight", as in Fig.1(b), and "stretched coils" as B in (c) only occur transiently. See also [Sta01] for an overview of these results.

Further experiments on coiling are discussed in [PQAEM09], with various hypothesis for the underlying mechanism, and [HEJ+14] discusses the role of the actin cortex (not considered in (5)) in suppressing pearling in actual cells. In [NSS15], tubular vesicles modeled by (1) with $c_0 = 0$ and $\mathcal{A}$ and $\mathcal{V}$ conservation, are subjected to external elongational and compressional flows, and numerical simulations are compared to experimental results. Depending on flow parameters (condensed to the capillary number), and the initial vesicle shape (including, e.g., the shape of the spherical caps at the ends of finite cylinders), pearling is observed for elongational flows, and buckling and coiling (called wrinkling in [NSS15]) for compressional flows. This is also complemented by linear stability analysis for infinite cylinders.

c) In our model (5) we do not consider any interaction with surrounding fluids; we treat the idealized infinitely long cylinders, or the idealization of a fixed spatial periodicity; and c_0 and the surface tension λ_1 and pressure difference λ_2 are always global. Hence, mismatches to experiments (small range of stability for periodic pearling, long wave nature of the buckling and coiling, see below) are not completely surprising, but we believe/hope that our analytical (instabilities of $\mathcal{C}_L$, derivation of the AEs) and numerical (continuation of the bifurcating branches to larger amplitude) discussion of (5) will also help the further modeling. ⌋

Outline, and overview of results. In §2 we recall the needed differential geometry and rewrite (5) as an equation in the normal displacement u from the cylinder. This gives a constrained quasi-linear parabolic problem in u, for which we use maximal regularity in Sobolev spaces to obtain local existence close to $\mathcal{C}_L$. From this we also obtain that nonlinear stability follows from linearized stability, and since $\mathcal{C}_L$ has constant mean and Gauß curvatures, the eigenvalues and eigenfunctions of the linearized problem can be computed explicitly allowing an analytical treatment of the instabilities of $\mathcal{C}_L$, and of the bifurcating branches via amplitude equations in §3 and §4. This is straightforward,

but cumbersome due to the three parameters c_0, L and λ_2, and requires a careful look at the area and volume constraints (2) already in the linearization. One result is that the coiling/buckling instability of $\mathcal{C}_L$ is always of long wave type, i.e., the primary coiling/buckling instability has the maximal period given by the length L, but for some (positive) c_0 the primary pearling instability can be of finite wave number type, i.e., independent of L. The wrinkling instability (homogeneous along the cylindrical axis) naturally is also independent of L. Then again due to the constraints in particular the derivation and interpretation of the AEs is non–standard.

In §5 we complement our analysis with numerical continuation and bifurcation methods, and also with some numerical flows for (5). As expected and already said, near bifurcation the numerics agree well with the analysis, but one remarkable result is that in case of finite wave number pearling the stability range of the bifurcating pearling branch rather strongly depends on L: The pearling branch becomes unstable via exchange of stability with a bifurcating branch of a "localized single pearl", and the associated bifurcation point moves closer to the primary bifurcation with increasing L. See §5 for details of this, and also for secondary bifurcations from other primary branches. In the Appendix we collect some details of the derivation of the AEs, and some remarks on the numerical algorithms.

2 Preliminaries and well-posedness of the flow

We introduce the basic differential geometric preliminaries in order to write (5) as a constrained parabolic quasi-linear equation in the normal displacement u of the cylinder. This construction is as in [LS16], and hence we refrain from extensive computational details and focus on the structure and mapping properties of the resulting equations. From these we obtain maximal regularity results and hence local existence for (5). For general background on differential geometry we recommend [Tap16, UY17].

2.1 Preliminaries

Let $\mathcal{C}(r)$ be the two dimensional unbounded cylinder embedded in $\mathbb{R}^3$ of radius $r > 0$ with the unbounded direction along the x axis. $\mathcal{C}(r)$ can be considered as the embedding

$$
\begin{aligned}
\Phi : \mathbb{R} \times \mathbb{T} &\to \mathbb{R}^3 \\
(x, \varphi) &\mapsto \big(x, r\cos(\varphi), r\sin(\varphi)\big)^T
\end{aligned}
\tag{8}
$$

of the product manifold $\mathbb{R} \times \mathbb{T}$, where $\mathbb{T}$ is the one dimensional topological torus with length 2π endowed with the metric $d_{\mathbb{T}}(\varphi, \vartheta) = \min\{|\varphi - \vartheta|, 2\pi - |\varphi - \vartheta|\}$ for all $\varphi, \vartheta \in \mathbb{T}$. Then as the pullback metric of the $\mathbb{R}^3$ to $\mathcal{C}(r)$ we have $g_0 = \mathrm{d}x^2 + r^2\,\mathrm{d}\varphi^2$. The normal vector (field) N of $\mathcal{C}(r)$ is oriented inwards, wrt Φ, hence $H(\mathcal{C}_r) = \frac{1}{2r}$.

For a function $u : \mathcal{C}(r) \to \mathbb{R}$, for the remainder of this subsection assumed as smooth as necessary, we consider surfaces

$$
X = \mathcal{C}(r) - u\,N,
$$

assuming $u < r$, such that X is still an embedding of $\mathbb{R} \times \mathbb{T}$; explicitly,

$$
\tilde{\Phi}(x, \varphi) = \Phi(x, \varphi) + \tilde{u}(x, \varphi)(0, \cos(\varphi), \sin(\varphi))^T,
$$

where $\tilde{u} = u \circ \Phi$. This gives the metric

$$
(g_{ij}) = \begin{pmatrix} 1 + u_x^2 & u_x u_\varphi \\ u_x u_\varphi & (r+u)^2 + u_\varphi^2 \end{pmatrix} \quad \text{with inverse } (g^{ij}) = \frac{1}{g}\begin{pmatrix} (r+u)^2 + u_\varphi^2 & -u_x u_\varphi \\ -u_x u_\varphi & 1 + u_x^2 \end{pmatrix}
$$

5

with $g = \det(g_{ij}) = (r+u)^2(1+u_x^2) + u_\varphi^2$. In the same explicit fashion one can calculate the second fundamental form

$$(h_{ij}) = \frac{1}{\sqrt{g}} \begin{pmatrix} (r+u)u_{xx} & (r+u)u_{x\varphi} - u_x u_\varphi \\ (r+u)u_{x\varphi} - u_x u_\varphi & (r+u)(u_{\varphi\varphi} - (r+u)) - 2u_\varphi^2 \end{pmatrix},$$

and this gives explicit formulas for the mean and Gaussian curvatures,

$$H(u) = \frac{1}{2g^{3/2}} \left(u_\varphi^2 - (r+u)\left[((r+u)^2 + u_\varphi^2)u_{xx} + (1+u_x^2)u_{\varphi\varphi} - 2u_x u_\varphi u_{x\varphi} \right] \right) + \frac{1}{2g^{1/2}}, \tag{9}$$

$$K(u) = \frac{1}{g^2} \left((r+u)u_{xx}\left[(r+u)(u_{\varphi\varphi} - (r+u)) - 2u_\varphi^2 \right] - \left((r+u)u_{x\varphi} - u_x u_\varphi \right)^2 \right). \tag{10}$$

We denote by Δ_g the negative definite Laplace–Beltrami operator

$$\Delta_u = \frac{1}{g^{1/2}} \left(\partial_x \left[\frac{(r+u)^2 + u_\varphi^2}{g^{1/2}} \partial_x - \frac{u_x u_\varphi}{g^{1/2}} \partial_\varphi \right] + \partial_\varphi \left[-\frac{u_x u_\varphi}{g^{1/2}} \partial_x + \frac{1+u_x^2}{g^{1/2}} \partial_\varphi \right] \right), \tag{11}$$

which is self adjoint in $L^2(X)$. Furthermore, the normal velocity is

$$V_t = -\left\langle \frac{\mathrm{d}}{\mathrm{d}t} X, N \right\rangle = \frac{(r+u)u_t}{g^{1/2}} = \eta(u)u_t \tag{12}$$

where $\eta(u) > 0$ for $u < r$, as we assumed. By all of this we can express (5) as a PDE in u, and with a slight abuse of notation we rewrite (5) as

$$\eta(u)\partial_t u = G(u, \Lambda), \tag{13a}$$
$$0 = q(u), \tag{13b}$$

where G has the quasi-linear structure $G(u, \Lambda) = B(u)u + C(u)$, where $B(u) = \sum_{|\alpha|=4} b_\alpha \partial_x^{\alpha_1} \partial_\varphi^{\alpha_2}$, where $b_\alpha = b_\alpha(u, \nabla u, \nabla^2 u)$, see (23), and where similarly C is a nonlinear operator of order up to three, but linear in the third derivatives.

Naturally, we shall need linearizations of (13) at $\mathcal{C}_L(r)$ and at $X(u) = \mathcal{C}_L(r) - uN$. For this we first note the formulas for derivatives of area $\mathcal{A}$ and volume $\mathcal{V}$, where we distinguish between the derivative of a functional $\mathcal{H}(u)$ acting on v in the L^2 scalar product, denoted by $\langle \partial_u \mathcal{H}, v \rangle$, and the integral kernel $\partial_u \mathcal{H}$ as a differential operator on X.

Lemma 2.1. *For $u, v \in C_{per}^\infty(\mathcal{C}_L(r))$ sufficiently small, the constraints (2) around $X(u) = \mathcal{C}_r - uN$ expand as $\mathcal{A}(u+v) = \mathcal{A}(u) + \langle \partial_u \mathcal{A}(u), v \rangle + O(\|v\|^2)$ with*

$$\langle \partial_u \mathcal{A}(u), v \rangle = 2 \int_X H(u)\eta(u)v \, \mathrm{d}S, \tag{14}$$

and second derivative at $\mathcal{C}_L$

$$\langle \partial_u^2 \mathcal{A}(0)v, v \rangle = \int_X -(\Delta_0 v + 2(H^2(0) - K(0))v)v \, \mathrm{d}S \tag{15}$$

and the volume

$$\mathcal{V}(u) = \frac{1}{2} \int_X \frac{(r+u)^2}{g^{1/2}(u)} \, \mathrm{d}S \tag{16}$$

expands as $\mathcal{V}(u + v) = \mathcal{V}(u) + \langle \partial_u \mathcal{V}(u), v \rangle + \frac{1}{2} \langle \partial_u^2 \mathcal{V}(u)v, v \rangle$ with

$$\langle \partial_u \mathcal{V}(u), v \rangle = \int_X \eta(u)v \, \mathrm{d}S, \quad \langle \partial_u^2 \mathcal{V}(u)v, v \rangle = \int_X g^{-1/2}(u)v^2 \, \mathrm{d}S. \tag{17}$$

Remark 2.2. Since Λ appears linearly in $G(u, \Lambda)$, the equation for the first derivative $\frac{\mathrm{d}}{\mathrm{d}t} q(u) = 0$ gives a linear system of equations

$$\mathcal{D}\Lambda = - \begin{pmatrix} \langle \partial_u E, \partial_u \mathcal{A}(u) \rangle \\ \langle \partial_u E, \partial_u \mathcal{V}(u) \rangle \end{pmatrix}, \tag{18}$$

for Λ, where

$$\mathcal{D} := \langle \partial_u q(u), \partial_\Lambda G(u, \lambda) \rangle = - \begin{pmatrix} 4 \int_X H^2(u)\eta^2(u) \, \mathrm{d}S & 2 \int_X H\eta^2(u) \, \mathrm{d}S \\ 2 \int_X H\eta^2(u) \, \mathrm{d}S & \int_X \eta^2(u) \, \mathrm{d}S \end{pmatrix}. \tag{19}$$

If $\det \mathcal{D} = 4 \left(\int_X \eta^2 \, \mathrm{d}S \int_X H^2 \eta^2 \, \mathrm{d}S + \left(\int_X H\eta^2 \, \mathrm{d}S \right)^2 \right) \neq 0$, then the implicit functions theorem gives that in a neighborhood of u there is a unique solution $\Lambda = \Lambda(u)$. Following [NY12], inserting $\Lambda(u)$ in (13a) gives a parabolic integro differential equation. However, if $u = 0$, then $\det \mathcal{D} = 0$, but the right hand side of (18) is orthogonal to $\ker \mathcal{D}$ (more generally, this holds at any constant mean curvature surface). Then a solution Λ to (18) exists, and $\langle \Lambda_\mathcal{C}, \ker \mathcal{D}^T \rangle = 0$ gives that $2\lambda_1 = \lambda_2$ and $\lambda_1 = \frac{1}{3\mathcal{A}_0} \langle \partial_u E, 1 \rangle$, i.e., $\ker \mathcal{D}$ corresponds to the family of cylinders in (7); see [NY12] for further discussion (for the case of closed vesicles of spherical topology).

Here we shall proceed similarly for the cylindrical vesicles; we start with well–posedness of (13a) for fixed $\Lambda \in \mathbb{R}^2$, i.e., with *inactive* constraints (13b). Then we first switch on one constraint, wlog $q_1(u) = 0$ and free $\lambda_1 = \lambda_1(t)$, and subsequently consider the full constraints $q(u) = (q_1(u), q_2(u)) = 0$ with free $\Lambda(t) = (\lambda_1(t), \lambda_2(t))$. ⌋

2.2 Well-posedness

Given an initial condition $u_0 \in \mathcal{X} \subset L^2(\mathcal{C}_L(r))$, i.e., $u_0 = u_0(x, \varphi)$ with periodic boundary conditions in x, where $\mathcal{X} = H^m_{\mathrm{per}}(\mathcal{C}_L(r))$ with the choice $m \in (3, 4)$ explained below, we search for solutions $(t, x, \varphi)) \mapsto (u(t, x, \varphi), \Lambda(t))$ of (13) on $[0, T) \times \mathcal{C}_r(L)$. Here $\mathcal{C}_L(r)$ is topologically equivalent to a torus, and the periodic Sobolev spaces of order $m \geq 0$ are

$$H^m_{\mathrm{per}} = H^m_{\mathrm{per}}(\mathcal{C}_L(r)) = \{v \in L^2(\mathcal{C}_L(r)) : \sum_{k \in \frac{2\pi}{L}\mathbb{Z} \times \mathbb{Z}} (1 + |k|^2)^m |\hat{v}_k|^2 < \infty\}, \tag{20}$$

where $\hat{v}_k = \langle v, e^{ik \cdot (x, \varphi)} \rangle$. Clearly, $H^{m_1}_{\mathrm{per}} \subset H^{m_2}_{\mathrm{per}}$ for $m_1 \geq m_2$, and $[H^{m_1}_{\mathrm{per}}, H^{m_2}_{\mathrm{per}}]_\theta = H^{(1-\theta)m_1 + \theta m_2}_{\mathrm{per}}$ for the associated real interpolation spaces, see [LM72] and [Tri78, §2.4.2], and $\nabla \in \mathcal{L}(H^m_{\mathrm{per}}, H^{m-1}_{\mathrm{per}})$.

In the following, for $m > 1$ we restrict the Sobolev spaces to open subsets

$$V^m_\varepsilon := H^m_{\mathrm{per}}(\mathcal{C}_L(r)) \cap \{|u| < r - \varepsilon\} \tag{21}$$

with some $0 < \varepsilon < r$. Then $\mathcal{C}_L(r) - uN$ is an embedding of $\mathcal{C}_L(r)$, and we can easily state local Lipschitz properties of the operators involved in (13). For convenience we recall some Sobolev embedding results, which hold for compact manifolds with boundary as for compact domains in $\mathbb{R}^n$, see, e.g., [Aub82].[3]

---

[3]The situation of non compact manifolds is more complicated, but if the manifold is complete, has a positive injection radius and bounded sectorial curvature, then the same results holds as well. In fact, in the following analysis near $\mathcal{C}_L(r)$ we do not strictly need the manifold versions of Sobolev embeddings due to the global coordinates (8) also underlying

In 2D, $H^m(X) \hookrightarrow L^\infty(X)$ for $m > 1$ embeds continuously, while $H^1(X)$ does not. Also, for $m = 1+\alpha$, $H^m(X) \hookrightarrow C^{0,\alpha}(X)$, hence the point evaluation $u(x,\phi)$ and in particular the sets $\{|u(x,\varphi)| < r - \varepsilon\}$ are well defined for $m > 1$.

2.2.1 Well-posedness of the PDE part

Following Remark 2.2 we first consider the PDE part (13a) with fixed $\Lambda \in \mathbb{R}^2$, i.e.,

$$\eta(u)\partial_t u = B(u)u + C(u), \tag{22}$$

where $B(u)$ collects the 4th order derivatives $b_{\alpha_1,\alpha_2}(u)\partial_x^{\alpha_1}\partial_\phi^{\alpha_2}$, $|\alpha| := \alpha_1 + \alpha_2 = 4$, namely

$$
\begin{aligned}
&b_{4,0}(u) = g^{-2}((r-u)^2 + u_\phi^2)^2, \quad b_{3,1}(u) = -g^{-2}(4u_x u_\phi((r+u)^2 + u_\phi^2), \\
&b_{2,2}(u) = g^{-2}(2((r-u)^2 + u_\phi^2)(1 + u_\phi^2) + 4u_x^2 u_\phi^2, \\
&b_{1,3}(u) = -4g^{-2}(u_x u_\phi(1 + u_x^2), \quad b_{0,4} = g^{-2}(1 + u_x^2)^2,
\end{aligned}
\tag{23}
$$

cf.[LS16], where our $B(u)$ appears as the principal part of the 4th order operator $P(u)$ in [LS16]. In particular, the symbol $\sigma[B(u)](x,\phi,\xi)$ satisfies

$$\sigma[B(u)](x,\phi,\xi) \geq g^{-2}((r-u)^2\xi_1^2 + \xi_2^2)^2, \tag{24}$$

and hence $B(u)$ is uniformly elliptic (in the 4th order sense) for $\|u\|_\infty < r - \varepsilon$, i.e. there exists constants c_1, c_2 such that $c \leq \sigma[B(u)](x,\phi,\xi) \leq C$ for all $(x,\phi,\xi) \in \mathcal{C}_L \times \mathbb{R}^2$ with $\|\xi\| = 1$.

We want to apply [MRS13, Theorem 3.1], which treats abstract quasilinear parabolic problems of the form

$$\partial_t u = A(u)u + F(u), \quad t > 0, \quad u(0) = u_0 \in \mathcal{X}, \tag{25}$$

with Gelfand triple $X_0 \hookrightarrow \mathcal{X} \hookrightarrow X_1 = D(A(u))$, i.e., phase space $\mathcal{X}$. For this we could rewrite (22) as $\partial_t u = \widetilde{B}(u)u + \widetilde{C}(u)$ with $\widetilde{B}(u) = \eta(u)^{-1}B(u)$ and $\widetilde{C}(u) = \eta(u)^{-1}C(u)$, but since $\eta(u) = (1 + u)g^{-1/2}$ contains at most first derivatives it will be clear from the following that we can as well keep $\eta(u)$ in (22) on the lhs and consider the rhs of (22) in the setting of (25). As already indicated above, we choose the base space $X_0 = L^2$ and hence $X_1 = D(B(u)) = H^4$, and we need to find an open subset $V = V_\varepsilon^m$ of the phase space $\mathcal{X}$ with $X_0 \subset \mathcal{X} \subset X_1$ such that

(W1) $B : V \to L(X_1, X_0)$ and $C : V \to X_0$ are locally Lipschitz;
(W2) for all $u \in V$, $B(u)$ generates a C_0 (strongly continuous) analytic semigroup in X_0.

By [MRS13, Theorem 3.1], (22) is then locally well posed in V, i.e., there exists a $t_0 > 0$ and a unique solution $u \in C([0,t_0), V) \cap H^1((0,t_0), X_0) \cap L^2((0,t_0), H^4)$. To show (W1) we use Sobolev embeddings and the structures of B and C, while (W2) essentially follows from (24).

Lemma 2.3. *For $m \in (3,4)$, $B(\cdot) \in C^\infty(V_\varepsilon^m, \mathcal{L}(H_{per}^4, L^2))$ and $C \in C^\infty(V_\varepsilon^m, L^2)$. In addition, the rhs of (13) is an analytic map from $V_\varepsilon^4 \times \mathbb{R}^2$ into L^2.*

Proof. From the Sobolev embeddings, a function $F(u) = u^j$ is well defined for any j on H^m if $m > 1$, and the map $u \mapsto g(u)$ is smooth from $H^m(X)$ to $H^{m-1}(X)$ for $m > 2$, and on V^m bounded away from zero. Hence $g^{-s} \in L^\infty(X)$ for $s > 0$ and due to the embedding $L^\infty(X) \hookrightarrow L^2(X)$, these terms are bounded in L^2. For u small enough g^{-s} can be expanded into a convergent power series, which gives the analyticity.

The coefficients (23) of $B(u)$ are well defined for $u \in V_\varepsilon^m$ with $m > 3$ since $u, \partial_x u, \partial_\phi u \in L^\infty$. Actually, $m > 2$ is enough here, and the condition $m > 3$ comes from $C(u)$, which has summands

---

(20), and hence we basically state the more general embedding results for possible generalization to other manifolds.

$c_\alpha(u, \nabla u, \nabla^2 u) = \tilde{c}_\alpha u^{j_1}(\partial_x u)^{j_2}(\partial_\varphi u)^{j_3}(\partial_x^2 u)^{j_4}(\partial_\varphi^2 u)^{j_5}(\partial_x \partial_\varphi u)^{j_6} g^{-s}(u, \nabla u)$, (nonlinear terms up to second order), and $d_\alpha(u, \nabla u)\partial_{x,\phi}^\alpha u$, $|\alpha| = 3$, where d_α is nonlinear but the third order terms (from $\Delta H(u)$ with $H(u)$ from (9)) only appear linearly. The maps $b_\alpha(u, y)$ are analytic on $\{|u| < r - \varepsilon\} \times \mathbb{R}^2$, and so are the $c_\alpha(u, y, z)$ on $\{|u| < r - \varepsilon\} \times \mathbb{R}^2 \times \mathbb{R}^4$, and the d_α on $\{|u| < r - \varepsilon\} \times \mathbb{R}^2$. By introducing a perturbation $u + \delta v$ for $v \in H^\alpha$, and computing the derivative wrt δ, we have, e.g.,

$$\partial_u c_\alpha(u, \nabla u, \nabla^2 u) = (\partial_x c_\alpha(x, y, z)v + \partial_y c_\alpha(x, y, z) \cdot \nabla v + \partial_z c_\alpha(x, y, z) \cdot \nabla^2 v)|_{(x,y,z)=(u,\nabla u, \nabla^2 u)}.$$

The structure of $\partial_u c_\alpha$ is hence the same as that of c_α, and similar for the b_α and d_α such that these "coefficients" respectively summands are well defined and finite in L^∞. This can be iterated for higher derivatives, to find the same result, and, e.g., for $w \in H^4$ and $u \in V_\varepsilon^m$,

$$\|\partial_u B(u)w\|_{L^2} \leq C\|w\|_{H^4}.$$

This gives the first two assertions, and setting $u = w$ gives the analyticity of $G(u, \Lambda)$, where the analyticity with respect to Λ is clear since Λ appears linearly. $\qquad\square$

To show (W2) we use standard theory for sectorial operators [Hen81, Lun95]. Let $u \in V_\varepsilon^m$. Since $D(B(u)) = H^4$ is dense in $X = L^2$, it is sufficient to show that $B(u)$ is sectorial in L^2, i.e., that the spectrum of $B(u)$ is contained in a sector $S_{\alpha,\omega}$ in $\mathbb{C}$ with tip at some $\omega \in \mathbb{R}$ of angle $\alpha < \pi$ opening to the left, and that there exists and $M > 0$ such that the resolvent estimate

$$\|(\lambda - B(u))^{-1}\| \leq \frac{M}{|\lambda - \omega|} \tag{26}$$

holds for all $\lambda \notin S_{\alpha,\omega}$. Essentially, this follows from the uniform ellipticity (24). In more detail, we show that $B(u)$ induces a coercive sesquilinear form on H^2, from which (W2) follows via the Lax–Milgram Lemma, see, e.g., [Sch24, Corollary 2.29].

Lemma 2.4. *For $u \in V_\varepsilon^m$ and λ sufficiently large, the operator $(\lambda - B(u))$ induces a coercive sesquilinear form on $H_{per}^2(\mathcal{C}_L(r))$, i.e., there exists ω, C independent of $u \in V_\varepsilon^m$ such that for $\lambda > \omega$ we have*

$$\int_{\mathcal{C}_r(L)} ((\lambda w - B(u)w)w \, dS \geq C\|w\|_{H_{per}^2(\mathcal{C}_r(L))}^2. \tag{27}$$

Proof. The idea is to use (24), but since $B(u)$ is not in divergence form we need to apply the standard trick of writing, e.g.,

$$b_{4,0}(u)\partial_x^4 w = \partial_x^2(b_{4,0}(u)\partial_x^2 w) - \partial_x(\widetilde{b}_{4,0}(u)\partial_x^2 w),$$

where $\widetilde{b}_{4,0}(u) = \partial_x b_{4,0}(u)$ is still bounded in L^∞, i.e., $\|\widetilde{b}_{4,0}(u)\|_\infty \leq C_{4,0}$. Therefore, using $|w_{xx} w_x| \leq \frac{\delta_1}{2}w_{xx}^2 + \frac{1}{2\delta_1}w_x^2$, $\delta_1 > 0$, and similarly standard L^2–interpolation estimates such as $\int_{\mathcal{C}_L(r)} w_x^2 \, dS \leq \int_{\mathcal{C}_L(r)} \frac{\delta_2}{2}w_{xx}^2 + \frac{1}{2\delta_2}w^2 \, dS$, we obtain, e.g.,

$$\langle(\lambda - b_{4,0}(u))w, w\rangle = \lambda \int w^2 \, dS + \int b_{4,0}(u)w_{xx}^2 + \widetilde{b}_{4,0}(u)w_{xx}w_x \, dS$$

$$\geq \left(c_1 - \frac{1}{2}(\delta_1 + \frac{\delta_2}{\delta_1})\right) \int w_{xx}^2 \, dS + \left(\lambda - \frac{C_{4,0}}{4\delta_1\delta_2}\right) \int w^2 \, dS,$$

with $c_1 > 0$ from (24). Proceeding similarly for the other terms from (23) and choosing suitable $\delta_{1,2}$ and then ω sufficiently large yields (27), uniformly in $u \in V_\varepsilon^m$. $\qquad\square$

9

In summary we have verified (W1) and (W2) with $V = V_\varepsilon^m$ with $m \in (3, 4)$ corresponding to $\vartheta \in (3/4, 1)$ for the interpolation space $[L^2, H^4]_{\vartheta,2} = H^m$, and we can apply [MRS13, Theorem 3.1] to obtain local existence for (22).

Theorem 2.5. *Let $m \in (3, 4)$ and fix $\Lambda \in \mathbb{R}^2$. Then for all $u_0 \in V_\varepsilon^m$ there exists a $t_0 = t_0(u_0)$ and a unique solution $u(\cdot, u_0) \in L^2((0, t_0), H^4(\mathcal{C})) \cap H^1((0, t_0), L^2(\mathcal{C})) \cap C([0, t_0], V_\varepsilon^m))$ of (22).*

2.2.2 The constrained flows

Following Remark 2.2, in order to take the constraints into account, we first consider only one active constraint namely $q_1(u) = 0$, and fix λ_2, while the same arguments also apply for the case of active q_2 with fixed λ_1. Defining $\overline{H} = \frac{H}{\|H\|_{L^2}}$ there exists a σ_1 such that $-(-\partial_u E + \lambda_2 \partial_u V + \lambda_1 H) = -(-\partial_u E + \lambda_2 \partial_u V + \sigma_1 \overline{H})$, and we define the projection $\mathcal{P}_1 : L^2(\mathcal{C}_r(L)) \to \text{span}\{\partial_u \mathcal{A}(u)\}^\perp$ by $\mathcal{P}_1 f = f - \langle \overline{H}, f \rangle \overline{H}$, and consider

$$V_t = \mathcal{P}_1(\partial_u E - \lambda_2 \partial_u V). \tag{28}$$

Then clearly $\frac{d}{dt}\mathcal{A}(u) = 2 \int_{\mathcal{C}_r(L)} H(u)V_t \, dS = 0$ and for $u \in V_\varepsilon^m$ we find

$$\lambda_1 = \frac{1}{\int_{\mathcal{C}_r(L)} H^2 \, dS} \langle \partial_u E - \lambda_2 \partial_u V, 2H \rangle = \frac{1}{\int_{\mathcal{C}_r(L)} H^2 \, dS} \int_{\mathcal{C}_r(L)} (\Delta H + 2H(H^2 - K) + c_0 K - 2c_0 H - \lambda_2 \partial_u V)H \, dS$$

$$= \frac{1}{\int_{\mathcal{C}_r(L)} H^2 \, dS} \int_{\mathcal{C}_r(L)} -|\nabla H|^2 + 2H^2(H^2 - K) + c_0 HK - 2c_0 H^2 - \lambda_2 \partial_u V H \, dS.$$

Importantly, the term $|\nabla H|^2$ includes third order derivatives of u but only quadratically in ∇H with lower order "coefficients" and hence $\int |\nabla H(u)|^2 \, dS$ is well defined and analytic for $u \in H_{\text{per}}^m$ for $m > 3$. This yields the analogous result as Theorem 2.5.

Theorem 2.6. *For $u_0 \in V_\varepsilon^m$ there exists a $t_0 = t_0(u_0)$ and a unique solution*

$$(u(\cdot, u_0), \lambda_1) \in (L^2((0, t_0), H^4(\mathcal{C})) \cap H^1((0, t_0), L^2(\mathcal{C})) \cap C([0, t_0), V_\varepsilon^s))) \times C([0, t_0), \mathbb{R}^1).$$

of $\eta(u)\partial_t u = G(u, (\lambda_1, \lambda_2))$ under the constraint $q_1(u) = \mathcal{A}(\mathcal{C}_L - uN) - \mathcal{A}_0 = 0$.

If $\det \mathcal{D}(u) \neq 0$, then we can consider the full constraints in (13) by projecting $V_t = \partial_u E$ onto the area and volume preserving flow. We construct an orthonormal basis of $\text{span}\{\partial_u \mathcal{A}, \partial_u V\} = \text{span}\{H, (r + u)g^{-1/2}(u)\}$ by Gram-Schmidt as

$$\overline{\partial_u V} = \frac{1}{\|\partial_u V\|_{L^2}}\partial_u V = \frac{1}{\|(r + u)g^{-1/2}(u)\|_{L^2}}(r + u)g^{-1/2}(u)$$

$$\overline{\partial_u \mathcal{A}} = \frac{1}{\|H - \langle \overline{\partial_u V}, H \rangle\|_{L^2}}(H - \langle \overline{\partial_u V}, H \rangle) = \frac{1}{\sqrt{\|H\|_{L^2}^2 - \langle \overline{\partial_u V}, H \rangle^2}}\left(H - \langle \overline{\partial_u V}, H \rangle\right).$$

We define the projection

$$\mathcal{P}_2 f = f - \langle \overline{\partial_u V}, f \rangle \overline{\partial_u V} - \langle \overline{\partial_u \mathcal{A}}, f \rangle \overline{\partial_u \mathcal{A}},$$

and obtain $\frac{d}{dt}\mathcal{A} = \langle \partial_u \mathcal{A}, V_t \rangle = 0$ and $\frac{d}{dt}V = \langle \partial_u V, V_t \rangle = 0$ for the flow $V_t = \mathcal{P}_2 \partial_u E$. Since $\det \mathcal{D}(u) \neq 0$, (18) is uniquely solvable also in a small neighborhood of u. So by inverting $\mathcal{D}(u)$ the Lagrange multipliers are

$$\lambda_1 = \frac{1}{\det \mathcal{D}}\left(\langle \partial_u V, \partial_u V \rangle \langle \partial_u E, \partial_u \mathcal{A} \rangle - \langle \partial_u \mathcal{A}, \partial_u V \rangle \langle \partial_u E, \partial_u V \rangle\right)$$

10

$$\lambda_2 = \frac{1}{\det \mathcal{D}} \left(\langle \partial_u \mathcal{V}, \partial_u \mathcal{V} \rangle \, \langle \partial_u E, \partial_u \mathcal{V} \rangle - \langle \partial_u \mathcal{A}, \partial_u \mathcal{V} \rangle \, \langle \partial_u E, \partial_u \mathcal{A} \rangle \right)$$

Recall that $\partial_u \mathcal{A} = 2H(u)\eta(u)$, that $\partial_u \mathcal{V}$ is of first order in u, and that the leading term in $\partial_u E$ is $\Delta H(u)$. Using integration by parts we find that the only term involving third order derivatives is $|\nabla H|^2$, which was already discussed. Hence we obtain the following result.

Theorem 2.7. *For $u_0 \in V_\varepsilon^m$ there exists a $t_0 = t_0(u_0)$ and a unique solution of (13),*

$$(u(\cdot, u_0), \Lambda(\cdot, u_0)) \in (L^2((0, t_0), H^4(\mathcal{C})) \cap H^1((0, t_0), L^2(\mathcal{C}) \cap C([0, t_0), V_\varepsilon^s))) \times C([0, t_0), \mathbb{R}^2).$$

3 Stability of $\mathcal{C}_L$

3.1 Linearization and eigenvalues

We consider the linearization of (5) around $\mathcal{C}_L(r)$. Since $G(\cdot, \Lambda) : V_\varepsilon^4 \to L^2$ is an analytic map, we use (9), (10) and (11) to calculate the Frechét derivative via the Gateaux differential in direction v, i.e., $\partial_u G(0, \Lambda)v = \frac{d}{d\varepsilon} G(\varepsilon v, \Lambda)|_{\varepsilon=0}$.

Lemma 3.1. *The linearizations of $H(u), K(u)$, and $\Delta_u H(u)$ around $\mathcal{C}_L(r)$, i.e., around $u = 0$, are given by*

$$\partial_u H(0)v = -\frac{1}{2}\left(\Delta_0 v + \frac{1}{r^2} v \right), \tag{29}$$

$$\partial_u K(0)v = -r^{-1}\partial_x^2 v, \text{ and} \tag{30}$$

$$\partial_u \Delta_0 H(0)v = \Delta \partial_u H(0)v. \tag{31}$$

Proof. First recall that $\Delta_0 = \partial_x^2 + \frac{1}{r^2}\partial_\varphi^2$, the Laplace-Beltrami operator on $\mathcal{C}_r$. Using (9) with εh and sorting by ε powers gives

$$H(\varepsilon h) = -\frac{\varepsilon(r^3 h_{xx} + r h_{\varphi\varphi}) + O(\varepsilon^2)}{(r^2 + \varepsilon 2rh + O(\varepsilon^2))^{3/2}} - \frac{1}{(r^2 + \varepsilon 2rh + O(\varepsilon^2))^{1/2}}.$$

Differentiating w.r.t. ε this gives

$$\frac{d}{d\varepsilon} H(\varepsilon h) = -\frac{(r^3 h_{xx} + r h_{\varphi\varphi})(r^2 + O(\varepsilon))^{3/2} + O(\varepsilon)}{(r^2 + \varepsilon 2rh + O(\varepsilon^2))^3} - \frac{rh}{(r^2 + O(\varepsilon))^{3/2}}.$$

The denominators are bounded away from zero, hence evaluating at $\varepsilon = 0$ gives (29).

For K this works the same way, with

$$\frac{d}{d\varepsilon} K(\varepsilon h) = \frac{d}{d\varepsilon} \frac{-\varepsilon r^3 h_{xx} + O(\varepsilon^2)}{(r^2 + 2\varepsilon 2rh + O(\varepsilon^2))^2} = \frac{-r^3 h_{xx}((r^2 + \varepsilon 2rh + O(\varepsilon^2))^2 + O(\varepsilon)}{(r^2 + \varepsilon 2rh + O(\varepsilon^2))^4}.$$

Again evaluating at $\varepsilon = 0$ gives (30).

Finally for (31) it is sufficient to notice that

$$\frac{d}{d\varepsilon} \Delta_{\varepsilon h} H(\varepsilon h)|_{\varepsilon=0} = \left(\frac{d}{d\varepsilon} \Delta_{\varepsilon h} H(0) \right)\bigg|_{\varepsilon=0} + \Delta_0 \left(\frac{d}{d\varepsilon} H(\varepsilon h)\bigg|_{\varepsilon=0} \right) = \Delta_0 \left(\frac{d}{d\varepsilon} H(\varepsilon h)\bigg|_{\varepsilon=0} \right),$$

since $H(0)$ is a constant and $\Delta_{\varepsilon h}$ is non degenerate for small perturbations. $\qquad \square$

Inserting the expressions from Lemma 3.1 we obtain

Lemma 3.2. $G(\cdot, \Lambda)$ *is Frechet differentiable at* $u = 0$, *with differential, using (7),*

$$\partial_u G(0, \Lambda) v = -\frac{1}{2} \Delta_0^2 v - \left(r\lambda_2 + \frac{1}{r^2}\right) \Delta_0 v - \left(\frac{\lambda_2}{r} + \frac{1}{2r^4}\right) v + \left(\frac{1}{r} - 2c_0\right) r^{-1} \partial_x^2 v. \tag{32}$$

Over the unbounded $\mathcal{C}(r)$, $\partial_u G(0, \Lambda))$ has a continuous spectrum, but by restricting to the compact cylinder $\mathcal{C}_L(r)$ of length L, $\partial_u G(0, \Lambda))$ has a discrete spectrum with a simple basis of eigenfunctions.

Lemma 3.3. *The eigenvalue equation*

$$\partial_u G(0, \Lambda) \psi = \mu \psi \tag{33}$$

has a countable set of solutions $(\mu_{mn}, \psi_{mn}) \in \mathbb{R} \times H_{per}^4(\mathcal{C}_L(r))$, $(m, n) \in \mathbb{Z}^2$,

$$\psi_{mn}(x, \varphi) = e^{\mathrm{i}(k_m x + n\varphi)}, \ k_m = 2m\pi/L, \ \text{with} \tag{34a}$$

$$\mu(m, n, \Lambda) = -\frac{1}{2}\left[k_m^2 + \frac{n^2}{r^2}\right]^2 + \left(r\lambda_2 + \frac{1}{r^2}\right)\left[k_m^2 + \frac{n^2}{r^2}\right] - \left(\frac{\lambda_2}{r} + \frac{1}{2r^4}\right) - \left(\frac{1}{r} - 2c_0\right)\frac{k_m^2}{r}. \tag{34b}$$

For all $\Lambda \in \mathbb{R}^2$ *the eigenfunctions* $\psi_{0\pm1} \in \ker(\partial_u G(0, \Lambda))$.

Proof. Recall that $H_{per}^4(\mathcal{C}_L(r))$ has a compact embedding in $L^2(\mathcal{C}_L(r))$, hence the resolvent of (32) is compact. Using the L^2 basis of eigenfunctions of Δ_0,

$$\psi_{mn}(x, \varphi) = e^{\mathrm{i}(k_m x + n\varphi)}, \quad \Delta_0 \psi_{mn} = -\left[k_m^2 + \frac{1}{r^2}n^2\right]\psi_{mn}(x, \varphi),$$

we obtain $\mu = \frac{1}{2}\left[k_m^2 + \frac{1}{r^2}n^2\right]^2 + \left(r\lambda_2 + \frac{1}{r^2}\right)\left[k_m^2 + \frac{1}{r^2}n^2\right] - \left(\frac{\lambda_2}{r} + \frac{1}{2r^4}\right) - \frac{1}{r}\left(\frac{1}{r} - 2c_0\right)r^{-1}k_m^2$, hence (34) after some rearranging. Clearly $\mu(0, \pm1, \Lambda) = 0$, hence $\sin(\varphi), \cos(\varphi) \in \ker(\partial_u G(0, \Lambda))$. $\square$

Using Lemma 2.1, we write the linearization of (13) as

$$\partial_U \mathcal{G}(0, \Lambda) U = \begin{pmatrix} \partial_u G(0, \Lambda) & \partial_{\lambda_1} G(0, \Lambda) & \partial_{\lambda_2} G(0, \Lambda) \\ \partial_u \mathcal{A}(0) & \partial_{\lambda_1} \mathcal{A}(0) & \partial_{\lambda_2} \mathcal{A}(0) \\ \partial_u \mathcal{V}(0) & \partial_{\lambda_1} \mathcal{V}(0) & \partial_{\lambda_2} \mathcal{V}(0) \end{pmatrix} \begin{pmatrix} u \\ \sigma_1 \\ \sigma_2 \end{pmatrix}$$

$$= \begin{pmatrix} \partial_u G(0, \Lambda) u & -2H(0)\sigma_1 & -\sigma_2 \\ -\int_{\mathcal{C}_L(r)} 2H(0) u \, \mathrm{d}S & 0 & 0 \\ \int_{\mathcal{C}_L(r)} u \, \mathrm{d}S & 0 & 0 \end{pmatrix}. \tag{35}$$

The domain of $\partial_U \mathcal{G}(0, \Lambda)$ is $H_{per}^4(\mathcal{C}_L(r)) \times \mathbb{R}^2$, equipped with the norm $\|U\|_{\partial_{(u,\Lambda)}\mathcal{G}} = \|u\|_{H^4} + \|\Sigma\|_{\mathbb{R}^2}$, and altogether we have the generalized eigenvalue problem $\Psi = (\psi, \sigma_1, \sigma_2)$

$$\partial_U \mathcal{G}(0, \Lambda) \Psi = \mu \begin{pmatrix} 1 & 0 & 0 \\ 0 & 0 & 0 \\ 0 & 0 & 0 \end{pmatrix} \Psi, \tag{36}$$

with eigenvalues $\mu \in \{\nu(m, n), (m, n) \in \mathbb{Z}^2 \backslash \{(0, 0)\} \cup \{0\}$ and eigenfunctions

$$\Psi_{m,n} = \begin{pmatrix} \psi_{m,n} \\ 1 \\ -2 \end{pmatrix}, \ (m, n) \in \mathbb{Z}^2 \backslash \{(0, 0)\}, \ \text{and} \ \Psi_{0,0} = \begin{pmatrix} 0 \\ 1 \\ -2 \end{pmatrix}.$$

12

Remark 3.4. (a) The eigenvalues $\mu(0, \pm 1, \lambda) = 0$ correspond to translations of $\mathcal{C}_L(r)$ in y and z directions. Each eigenvalue of the form $\mu(m, 0, \Lambda)$ and $\mu(0, n, \Lambda)$ has multiplicity two and every "double" eigenvalue $\mu(m, n, \Lambda)$ with $m \neq 0 \neq n$ has multiplicity four with eigenfunctions $\psi_{\pm m \pm n}$.

(b) The eigenvalues $\mu(m, n, \Lambda)$ do not explicitly depend on λ_1, but implicitly. Recall (7), which shows that the parameters are not independent at the cylinder.

(c) In the following we also use the notation $\Psi_{m,n}$ for the first two components of $\Psi_{m,n}$, which are the eigenvectors for the case of just the area constraint being active, cf. Theorem 2.6 and (37) in §3.2.

(d) The crucial difference of the spectrum of (36) and just the PDE part (33) is that $(\psi_{00}, 1, -2)$ with $\psi_{00} \equiv 1$ is not an eigenvector of $\partial_u \mathcal{G}(0, \Lambda)$. ⌋

3.2 Center manifold construction

At $\mathcal{C}_L(r)$, $\det \mathcal{D} = 0$, and we cannot perturb $\mathcal{C}_L(r)$ while preserving the area and the volume. Therefore we start with

$$\begin{pmatrix} \partial_t u \\ 0 \end{pmatrix} = \begin{pmatrix} \eta^{-1}(u) G(u, \Lambda) \\ q_1(u, \Lambda) \end{pmatrix} =: \mathcal{G}_{\mathcal{A}}(u, \Lambda), \tag{37}$$

where $\Lambda = (\lambda_1, \lambda_2)$ with λ_2 a *fixed* external pressure difference. The $\mathbb{R}^3$ has the Euclidean symmetry group $E(3)$ of rigid body motions, which can be constructed using two smooth curves $\tau, \varrho : \mathbb{R} \to \mathbb{R}^3$ with $\tau(0) = \varrho(0) = 0$, such that the translated and rotated surface is given by

$$\tilde{X} = \{y + \tau(\eta) + y \times \varrho(\eta) : y \in X\}.$$

However, since we only consider normal variations of X, admissible rigid body motions are

$$\mathcal{M}X = \{X + u\,N : u = \langle \tau(\eta) + y \times \varrho(\eta), N(y) \rangle\}.$$

The dimension of $\mathcal{M}X$ is given by the dimension of the tangent space $T_e \mathcal{M}X$ at the identity, hence spanned by $\langle \tau'(0), N(y) \rangle$ and $\langle y \times \varrho'(0), N(y) \rangle$. Since $\tau'(0)$ and $\varrho'(0)$ are arbitrary vectors,

$$T_e \mathcal{M}X = \mathrm{span}\{\langle e_i, N \rangle, \langle y \times e_i, N \rangle, \, i = 1, 2, 3\}. \tag{38}$$

But for $\mathcal{C}_L(r)$ we have

$$T_e \mathcal{M}\mathcal{C}_r = \mathrm{span}\{\langle e_2, N \rangle, \langle e_3, N \rangle\} = \mathrm{span}\{\psi_{01}, \psi_{0-1}\} \tag{39}$$

where a straightforward calculation shows that translation in and rotation around e_1 generate tangential motions to $\mathcal{C}_L(r)$, while rotations around e_2 and e_3 violate the periodicity in x.

In §3.3 we will see that there are parameter values λ_2 such that the spectrum of the linearization of (37) is contained in the negative half plane, with one zero eigenvalue with multiplicity according to (39). The spectrum on the finite cylinder is discrete, with a spectral gap between the zero and first non zero eigenvalue. Hence the spectrum decomposes into the center spectrum spec_c and the stable spectrum spec_s. Using the well-posedness Theorem 2.6 we may apply [Sim95, Theorem 4.1] on the existence of a center manifold under the above conditions. Since (39) shows that the center eigenspace coincides with the tangent space of the manifold of translated cylinders, both manifolds also coincide locally. This gives the following results.

Lemma 3.5. *At the trivial solution $(0, \lambda_2)$ with λ_1 and λ_2 related by (7), there exists a smooth center manifold $\mathcal{M}^c$ for (37) at least of dimension two. If the kernel of $\partial_{(u, \lambda_2)} \mathcal{G}_{\mathcal{A}}$ is spanned by $\Psi_{0 \pm 1}$ then*

$$\mathcal{M}^c = \text{Shifts in } y \text{ and } z \text{ direction.} \tag{40}$$

Theorem 3.6. *If $\lambda_2 \in \mathbb{R}$ such that the spectrum of $\partial_{(u,\lambda_2)}\mathcal{G}_\mathcal{A}$ is contained in $(-\infty, 0]$ and $\ker(\partial_{(u,\lambda_2)}\mathcal{G}_\mathcal{A})$ is spanned by $\Psi_{0\pm1}$, then there exist $\delta, \omega, M > 0$ such that for all $u_0 \in V_\varepsilon^m$ with $\|u_0\|_{H^m} < \delta$ the solution $U = (u, \lambda_1)$ of (37) exists globally in time and there exist a unique $U_\infty \in \mathcal{M}^c$ such that*

$$\|U(t, U_0) - U_\infty\|_{H^m \times \mathbb{R}} \leq M e^{-\omega t} \|U_0\|_{H^m \times \mathbb{R}}.$$

3.3 Stability and instability

Following Theorem 3.6, to check for stability of $\mathcal{C}_L(r)$ we seek $\Lambda \in \mathbb{R}^2$ such that all eigenvalues $\mu(m, n, \Lambda)$ are in $(-\infty, 0]$, and the only zero eigenvalues belong to $\Psi_{0\pm1}$ (translations in y and z). *From here on, to simplify notation we fix $r = 1$.* Practically, we vary λ_2 along the trivial branch, and monitor the signs of the eigenvalues. Due to the three parameters (L, c_0, λ_2), with λ_1 given by (7), we will distinguish between several cases, while the main questions are:
  - Are there intervals for λ_2 such that $\mathcal{C}_L$ is linearly stable?
  - Which modes destabilize the cylinder at what λ_2?

The zeros of μ give values $\lambda_2(m, n)$, indicating which mode induces the instability. Thus we compute the zeros of $\mu(m, n, \Lambda)$ and the slope $\partial_{\lambda_2}\mu(m, n, \Lambda)$, giving us on which side the eigenvalue is negative, splitting the (L, c_0) plane. As a visualization, Fig. 2 shows plots of the regions of stability (in green) and some spectral plots of selected dispersion relations.

For $m = 0$ we have

$$\mu(0, n, \Lambda) = -\frac{n^4}{2} + (\lambda_2 + 1)n^2 - \left(\lambda_2 + \frac{1}{2}\right), \tag{41}$$

with $\mu(0, \pm1, \Lambda) = 0$ for all Λ (translational eigenvalues), and

$$\partial_{\lambda_2}\mu(0, n, \Lambda) = n^2 - 1$$

is positive for $n > 1$. Furthermore μ is zero at $\lambda_2(0, n) = (1 - n^2)^{-1}(-\frac{n^4}{2} + n^2 - \frac{1}{2})$, which is monotonously increasing in n. Hence *under axially constant perturbations $\mathcal{C}_r$ is stable for $\lambda_2 < \frac{3}{2}$.*

Next we consider the modes $m \neq 0 \neq n$, in particular $(m, n) = (1, 1)$, where

$$\mu(1, 1, \Lambda) = -\frac{1}{2}((k_1^2 + 1)^2 + (\lambda_2 + 1)(k_1^2 + 1) - \left(\lambda_2 + \frac{1}{2}\right) - (1 - 2c_0)k_1^2$$

$$= -\frac{1}{2}(k_1^2 + 1)^2 + (\lambda_2 - 2c_0)k_1^2 + \frac{1}{2}.$$

One sees directly that $\mu(1, 1, \Lambda)$ is strictly increasing in λ_2 and has a zero for

$$\lambda_2^{(1,1)} = \frac{1}{2}k_1^2 + 1 - 2c_0, \tag{42}$$

where λ_2 is strictly decreasing in L because so is $k_m = 2m\pi/L$. Hence, *if $c_0 > -1/4$, then there exists an L large enough so that the cylinder destabilizes due to the $(m, n) = (1, 1)$ mode with L explicitly computable.*

For $m \geq 1$ and $n = 0$ (pearling), the eigenvalues

$$\mu(m, 0, \Lambda) = -\frac{1}{2}k_m^4 + (\lambda_2 + 2c_0)k_m^2 - \lambda_2 - \frac{1}{2}$$

behave as follows. Depending on L, either $k_m < 1$ such that $\mu(m, 0, \Lambda)$ is strictly decreasing in λ_2, or $k_m > 1$ such that $\mu(m, 0, \Lambda)$ is strictly increasing in λ_2. In either case, for $m = 1$ the eigenvalue has a
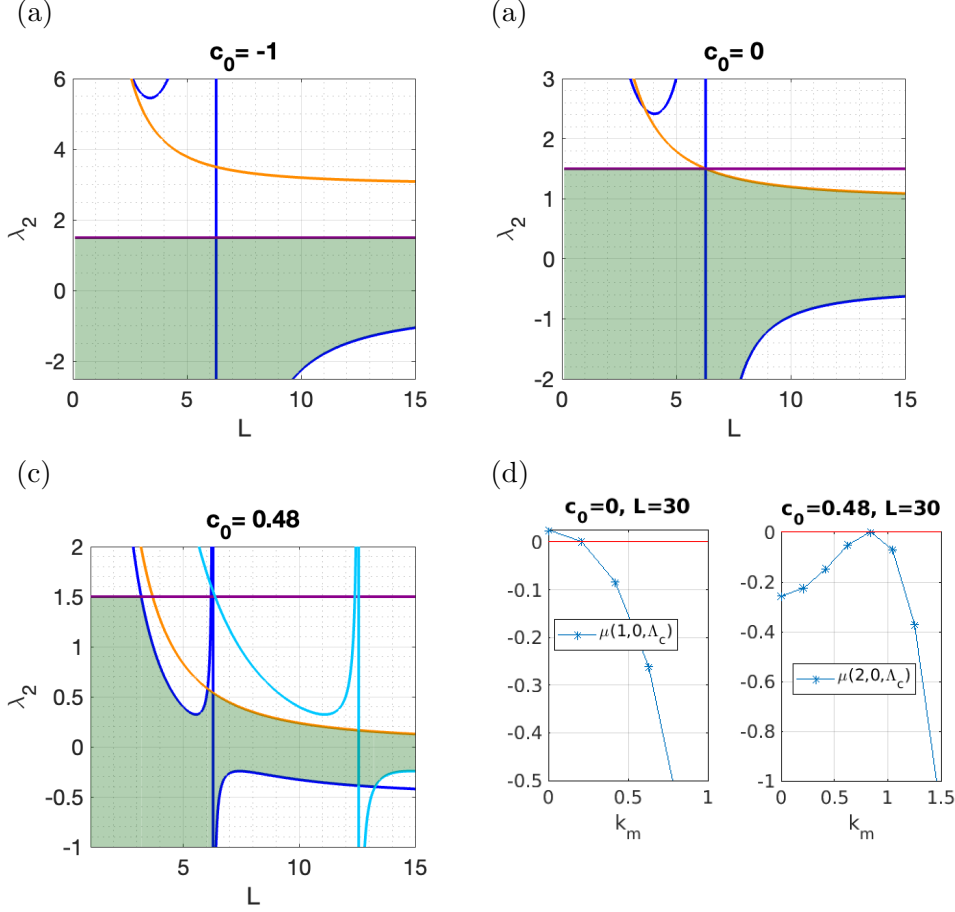
Figure 2: (a–c) Instability curves in the L–λ_2 plane (λ_1 according to (7)) for different values of c_0, delimiting the λ_2 parameter range for stability of $\mathcal{C}_L$. The blue curve correspond to the mode $(m,n) = (1,0)$ (minimal wave number pearling instability), the orange to $(m,n) = (1,1)$ (minimal wave number coiling/buckling) and the violet $\lambda_2 = 3/2$ to $(m,n) = (0,2)$ (wrinkling, independent of L). Lighter blue in (c) correspond to $(m,n) = (2,0)$, which gives the only finite wave number (independent of L) instability. (d) illustrates the long wave nature of the $(1,0)$ pearling instability at $(c_0,L) = (0,30)$ (as $k_m = 0$ is forbidden by the area (or volume) constraint, and the finite wave number nature of the $(2,0)$ pearling instability at $(c_0,L) = (0.48,30)$.

zero at

$$\lambda_2^{(m,0)} = \left[1 - k_m^2\right]^{-1} \left(-\frac{1}{2}k_m^4 + 2c_0 k_m^2 - \frac{1}{2} \right) \tag{43}$$

for all $L \in \mathbb{R}\backslash\{2\pi m\}$. First we note that the asymptote at $L = 2\pi m$ is odd, where for $c_0 < \frac{m}{2}$, $\lim_{k_m \searrow 1} \lambda_2 = -\infty$ and for $c_0 > \frac{m}{2}$ the other way around. In the latter case there always exists a L such that the m'th mode destabilizes the cylinder, so we do not focus further on that case. A straightforward analysis of (43) shows that it admits two positive solutions

$$L = \begin{cases} L_G = 2\pi \left(\frac{1+\sqrt{2}\sqrt{1-2c_0}}{4c_0-1}\right)^{1/2} & \text{for } c_0 \in (1/4, 1/2], \\ L_{S_1} = 2\pi \left(\frac{1-\sqrt{2}\sqrt{1-2c_0}}{4c_0-1}\right) & \text{for } c_0 \in (-\infty, 1/2], \\ L_{S_2} = \sqrt{2}\pi, & \text{for } c_0 = 1/4, \end{cases}$$

where for $i = 1, 2$ it holds that $L_{S_i} < 2\pi$ and are minima. For $c_0 \leq \frac{1}{2}$ and $L > 2\pi$ the eigenvalue $\mu(1, 0, \Lambda)$ has negative slope at (43), hence for smaller λ_2 the cylinder is destabilized. In the case of $c_0 \leq \frac{1}{4}$, λ_2 is monotonously increasing in L, yielding a maximum wavelength instability. In the regime where L_G exists, the $\mathcal{C}_L$ destabilizes to a finite wave length.

15

In the following Corollary of Theorem 3.6 we summarize the above, where maximal wave length (or long wave instability) refers to the minimal allowed $k_1 = 2\pi/L$, since $k_0 = 0$ is prohibited by the volume and area constraints.

Corollary 3.7. *The cylinder $\mathcal{C}_L$ is volume and area preserving stable for every $L > 0$ if:*

(a) $c_0 \in (1/4, 1/2)$ and $\lambda_2 \in (\lambda_2^{(1,0)}, \lambda_2^{(1,1)})$; $\mathcal{C}_L$ destabilizes at $\lambda_2^{(1,0)}$ with finite wave length L_G wrt the mode ψ_{20} (pearling), and at $\lambda_2^{(1,1)}$ wrt the mode ψ_{11} (buckling and coiling) of maximal wave length.

(b) $c_0 \in [-1/4, 1/4]$ and $\lambda_2 \in (\lambda_2^{(1,0)}, \lambda_2^{(1,1)})$; $\mathcal{C}_L$ destabilizes at $\lambda_2^{(1,0)}$ wrt to the mode ψ_{10} (pearling), and at $\lambda_2^{(1,1)}$ wrt the mode ψ_{11} (buckling and coiling), both of maximal wave length.

(c) $c_0 \in (-\infty, -1/4]$ and $\lambda_2 \in (\lambda_2^{(1,0)}, \lambda_2^{(0,2)})$; $\mathcal{C}_L$ destabilizes at $\lambda_2^{(1,0)}$ wrt the mode ψ_{10} (pearling) with maximal wave length, and at $\lambda_2^{(0,2)}$ wrt the mode ψ_{01} (wrinkling, homogeneous in x).

If $c_0 > 1/2$ there is always a positive eigenvalue for every λ_2, hence the cylinder is spectrally unstable.

4 Bifurcations from $\mathcal{C}_L$

We now compute the branches bifurcating at the instabilities given in Corollary 3.7. In §4.1 we give the general symmetry based bifurcation results, and in §4.2 we derive the associated amplitude equations and moreover discuss the stability of the bifurcating branches.

4.1 General bifurcation results

As a bifurcation problem, the desired primary bifurcation parameter is either $\mathcal{V}$ or $\mathcal{A}$. However, these parameters do not change along the trivial $u = 0$ branch, and therefore we first choose λ_2 as the primary bifurcation parameter and only consider (37), which we write as

$$\eta(u)\partial_t u = G(u, \Lambda), \tag{44a}$$

$$0 = \mathcal{A}(u) - \mathcal{A}_0. \tag{44b}$$

The linearization of (44) is the first 2×2 block of $\partial_U \mathcal{G}$, hence with eigenvalues (34) with $(m, n) \in \mathbb{Z}^2 \setminus \{(0,0), (0, \pm1)\}$, and eigenvectors

$$\Psi_{mn}(x, \varphi) = \begin{pmatrix} A_{mn} e^{i(k_m x + n\varphi)} + \text{c.c.} \\ 0 \end{pmatrix}. \tag{45}$$

Here μ_{00} is not present since it corresponds to changes of radius along the cylinder branch. Solving (2) gives (possible) bifurcation points (for completeness with r–dependence)

$$\lambda_2 = \left[\frac{(1 - n^2)}{r^2} - k_m^2 \right]^{-1} \left(-\frac{1}{2} \left[k_m^2 + \frac{n^2}{r^2} \right]^2 + \frac{1}{r^2} \left[k_m^2 + \frac{n^2}{r^2} \right] - \left(\frac{1}{r} - 2c_0 \right) \frac{k_m^2}{r} - \frac{1}{2r^4} \right). \tag{46}$$

Due to symmetries the bifurcation points have multiplicities at least two, and hence the equivariant branching lemma [CL00, GS02, Hoy06] gives the needed framework for the bifurcation analysis.

Theorem 4.1. *At (46) in the system (44) we have equivariant pitchfork bifurcations of steady state solutions $X(\varepsilon) = \mathcal{C}_r(L) - u(\varepsilon)N$, $\Lambda(\varepsilon) = \Lambda_0 + \mathcal{O}(\varepsilon^2)$, for some $0 < |\varepsilon| < \varepsilon_0$ sufficiently small. The maps $\varepsilon \mapsto (u(\varepsilon), \Lambda(\varepsilon)) \in H^4 \times \mathbb{R}^2$, or, equivalently $\varepsilon \mapsto (X(\varepsilon), \Lambda(\varepsilon)) \in H^4_{per}(\mathcal{C}_r(L), \mathbb{R}^3) \times \mathbb{R}^2$ are analytic, and we characterize the bifurcations as follows:*
(a) $n = 0$ (pearling):

$$u = \left(A_m e^{ik_m x} + \text{c.c.} \right) \varepsilon + \mathcal{O}(\varepsilon^2) \tag{47}$$

with some amplitude $A_m \in \mathbb{C}$, equivariant wrt translations in x.

(b) $m = 0$ *(wrinkling):*

$$u = \left(A_n e^{\mathrm{i}n\varphi} + \text{c.c.}\right)\varepsilon + \mathcal{O}(\varepsilon^2) \tag{48}$$

with some amplitude $A_n \in \mathbb{C}$, equivariant wrt rotations in φ.

(c) $m \neq 0 \neq n$ *(buckling and coils): Two types branches bifurcate. Buckling*

$$u = \left(A_{mn} e^{\mathrm{i}(k_m x + n\varphi)} + \text{c.c.}\right)\varepsilon + \mathcal{O}(\varepsilon^2), \tag{49}$$

equivariant wrt to translations in x and rotations in ϕ. The other branch are coils as equal amplitude superpositions of buckling,

$$u = \left(A_{mn} e^{\mathrm{i}(k_m x + n\varphi)} + A_{m-n} e^{\mathrm{i}(k_m x - n\varphi)} + \text{c.c.}\right)\varepsilon + \mathcal{O}(\varepsilon^2), \tag{50}$$

equivariant wrt to translations in x, or, equivalently wrt rotations in ϕ, which yield the same group orbit.

Proof. The proof proceeds via the equivariant branching lemma, see for example [CL00, Theorem 2.3.2]. By Equation 24, $B(u)$ is elliptic, hence the linearization of $G(u, \Lambda)$ is elliptic as well, and hence the upper left 2×2 block of $\partial_U \mathcal{G}$ is a Fredholm operator. At every λ_2 from (46), the zero eigenvalue is of finite multiplicity, namely multiplicity 2 in (a,b), and multiplicity 4 in (c), and the symmetries of the bifurcating branches are as follows:

(a) $X(\varepsilon)$ admits a new non trivial symmetry wrt translations in x. Assume that $A_{-m} = A_m$ with $A_m \in \mathbb{R}$, so that $u = \cos(k_m x)$. The (not normalized) normal vector is

$$\nu = \partial_x X(\varepsilon) \times \partial_\varphi X(\varepsilon) = \begin{pmatrix} 1 \\ -k_m \sin(k_m x)\cos(\varphi) \\ -k_m \sin(k_m x)\sin(\varphi) \end{pmatrix} \times \begin{pmatrix} 0 \\ -(1 + \cos(k_m x))\sin(\varphi) \\ (1 + \cos(k_m x))\sin(\varphi) \end{pmatrix}$$

$$= -(1 + \cos(k_m x)) \begin{pmatrix} k_m \sin(k_m x) \\ \cos(\varphi) \\ \sin(\varphi) \end{pmatrix}.$$

Hence $\langle \nu, e_j \rangle \neq 0$ for $j = 1, 2, 3$, hence $\text{span}\{\langle \nu, e_j \rangle\}$ is a subset of the generator of the center manifold of $X(\varepsilon)$. Following this with

$$X(\varepsilon) \times e_1 = \begin{pmatrix} 0 \\ -(1 + \cos(x))\sin(\varphi) \\ (1 + \cos(x))\cos(\varphi) \end{pmatrix},$$

we have that $\langle X(\varepsilon) \times e_1, \nu \rangle = 0$.

(b) As for (a) we can calculate the center manifold in the bifurcating branch, with

$$\nu = \partial_x X(\varepsilon) \times \partial_\varphi X(\varepsilon) = \begin{pmatrix} 0 \\ 2\sin(2\varphi)\sin(\varphi) + \cos(2\varphi)\cos(\varphi) \\ 2\sin(2\varphi)\cos(\varphi) + \cos(2\varphi)\sin(\varphi) \end{pmatrix}$$

and

$$\langle X(\varepsilon) \times e_1, \nu \rangle = \left\langle \begin{pmatrix} 0 \\ (1 + \cos(2\varphi))\sin(\varphi) \\ -(1 + \cos(2\varphi))\cos(\varphi) \end{pmatrix}, \nu \right\rangle = \cos(2\varphi)(1 + \cos(2\varphi))\cos(\varphi)\sin(\varphi).$$

17

Hence in the center manifold of $X(\varepsilon)$ are besides the translation in y and z direction also rotations around the x axis.

(c) The 4D kernel generates two different types of branches. For the coils we have

$$\partial_x X(\varepsilon) = \begin{pmatrix} 1 \\ 0 \\ 0 \end{pmatrix} - k_m \sin(k_m x + n\varphi) \begin{pmatrix} 0 \\ \cos(\varphi) \\ \sin(\varphi) \end{pmatrix}$$

$$\partial_\varphi X(\varepsilon) = (1 + \cos(k_m x + n\varphi)) \begin{pmatrix} 0 \\ -\sin(\varphi) \\ \cos(\varphi) \end{pmatrix} - n \sin(k_m x + n\varphi) \begin{pmatrix} 0 \\ \cos(\varphi) \\ \sin(\varphi) \end{pmatrix}$$

so the normal vector is

$$\nu = (1 + \cos(k_m x + n\varphi)) \begin{pmatrix} 0 \\ -\cos(\varphi) \\ -\sin(\varphi) \end{pmatrix} - n \sin(k_m x + n\varphi) \begin{pmatrix} 0 \\ -\sin(\varphi) \\ \cos(\varphi) \end{pmatrix}$$
$$- k_m \sin(k_m x + n\varphi)(1 + \cos(k_m x + n\varphi)) \begin{pmatrix} 1 \\ 0 \\ 0 \end{pmatrix}$$

Obviously, this results in a non trivial translational symmetry in x. Similarly

$$X(\varepsilon) \times e_1 = \begin{pmatrix} 0 \\ -(1 + \cos(k_m x + n\varphi))\sin(\varphi) \\ (1 + \cos(k_m x + n\varphi))\cos(\varphi) \end{pmatrix},$$

such that $\langle X(\varepsilon) \times e_1, \nu \rangle = n \sin(k_m x + n\varphi)(1 + \cos(k_m x + n\varphi))$ yields the same action as the translation. For the buckling solutions similar computations show that $\mathrm{span}\{\langle \nu, e_1 \rangle, \langle X(\varepsilon) \times e_1, \nu \rangle\}$ is two dimensional, hence the full symmetry is needed.

$\square$

4.2 Reduced equation

To further describe the bifurcations from Theorem 4.1, we derive the reduced equations (or amplitude equations AEs) at $\mathcal{C}_L$. These are straight forward computations, but somewhat cumbersome in our geometric setting and thus we partly use `Maple`. Here we explain the basic steps, and the computations for the pearling and wrinkling instability, but for the coils vs buckling we relegate some details to Appendix A.1. Additionally we give the numerical values of the coefficients of the AEs for some of examples, which will later be compared to numerics for the full problem.

According to Theorem 4.1, at "simple" (strictly speaking of multiplicity two, but from here we factor out the translation or rotation) bifurcation points (46), i.e., $(m, n) = (m, 0)$ or $(m, n) = (0, n)$, the bifurcating steady state branch is tangential to solutions of $D\mathcal{G}(0, \Lambda)[(\psi, 0)] = 0$ where $\mathcal{G}$ is the rhs of (44). We thus introduce the small parameter

$$\varepsilon = \sqrt{\left| \frac{\lambda_2 - \lambda_2(m, n)}{\beta_2} \right|}, \tag{51}$$

where $\beta_2 = \pm 1$ is introduced for later convenience to deal with sub–and supercritical pitchforks, and

altogether we use the ansatz

$$u = \varepsilon A \psi_{m,n} + \varepsilon^2 \sum_{(i,j) \in \mathcal{B}} A_{i,j} \psi_{i,j} + \text{c.c.} + \mathcal{O}(\varepsilon^3), \tag{52}$$

$$\lambda_2 = \lambda_2(m,n) + \beta_2 \varepsilon^2 + \mathcal{O}(\varepsilon^3), \quad \lambda_1 = \lambda_1(m,n) + \alpha_2 \varepsilon^2 + \mathcal{O}(\varepsilon^3), \tag{53}$$

where $\mathcal{B}$ is the index set of the modes generated from the critical modes in quadratic interactions, $A = A(T)$, $A_{i,j} = A_{i,j}(T)$, and $T = \varepsilon^2 t$. The $O(2) \times O(2)$ symmetry of the system (translations and reflections in x, and in φ, where for the simple bifurcations only one is nontrivial, translation for pearling, and rotation for wrinkles) is inherited by the reduced equation which hence has the form $\frac{\mathrm{d}}{\mathrm{d}T}A = Ag(A, \overline{A}, (\alpha_j)_{j=1,\dots,N-1}, (\beta_j)_{j=1,\dots,N-1})$, where g is an even function in all variables, i.e., in lowest order

$$\frac{\mathrm{d}}{\mathrm{d}T}A = A\left(a\beta_2 + b|A|^2\right). \tag{54}$$

At the "double" BPs $m \neq 0 \neq n$ two types of branches bifurcate, and we give the ansatz below.

Near a bifurcation point from a stable branch, the critical mode determines the evolution, while all others are exponentially damped. Hence, in a standard AE setting, the signs of a, β_2 and b in (54) determine the stability on the bifurcating branch. Here, from (54) we get stability information for steady states under area constraint, with λ_2 as extrinsic fixed parameter, but this can be extended to stability under area and volume constraints as follows. Close to the bifurcation point $\lambda_2(m,n)$ the solution reads $X(\varepsilon) = \mathcal{C}_L - \varepsilon A\psi N$. Then the solution is linearly stable iff $\partial_U \mathcal{G}(X(\varepsilon), \Lambda)$ (which includes the q_1 area constraint) has only negative eigenvalues. For admissible (area and volume preserving) perturbations $\phi : \mathcal{C}_L \to \mathbb{R}$ of $X(\varepsilon)$, we have the necessary and sufficient conditions

$$\int_{X(\varepsilon)} H(\varepsilon A\psi)\phi \, \mathrm{d}S = \int_{X(\varepsilon)} \varepsilon A\psi g^{-1/2}(\varepsilon A\psi)\phi \, \mathrm{d}S = 0.$$

For the mean curvature we have $H(\varepsilon A\psi) = \frac{1}{2} - \varepsilon A(\mu(m,n) + 1)\psi + \mathcal{O}(\varepsilon^2)$, and hence admissible perturbations must be orthogonal to ψ. Thus, near bifurcation points associated with loss of stability of $\mathcal{C}_L$ we have the following results:

- Branches bifurcating from simple bifurcation points (pearling or wrinkling), are stable wrt (5).
- Solutions on branches from a double bifurcation point (buckling and coiling), can only be destabilized by the other kernel vectors. We will see examples of this in §5.

4.2.1 Pearling instability

For the pearling instability (with for notational simplicity $m = 1$) we have

$$\varepsilon u = \varepsilon A \psi_{10} + \varepsilon^2 \left(\frac{1}{2}A_0\psi_{00} + A_2\psi_{20}\right) + \text{c.c.} + \mathcal{O}(\varepsilon^3), \quad \varepsilon = \sqrt{\left|\frac{\lambda_2(1,0) - \lambda_2}{\beta_2}\right|},$$

with $A = A(T)$, $T = \varepsilon^2 t$. Plugging into (44) and sorting by powers of ε, with the abbreviations $\lambda_2 = \lambda_2(1,0)$ and $k = k_1$, we obtain the following:

$\varepsilon\psi_{10} : 0 = -\frac{1}{2}\left(\left(k^4 + (-4c_0 - 2\lambda_2)k^2 + 2\lambda_2 + 1\right)\right)A.$

$\varepsilon^2\psi_{00} : 0 = \left(-\lambda_2 - \frac{1}{2}\right)A_0 + \frac{1}{2}\left(\left(k^4 + (-8c_0 - 2\lambda_2 - 1)k^2 + 4\lambda_2 + 5\right)|A|^2\right) - \beta_2 - \alpha_2.$

$\varepsilon^2\psi_{20} : 0 = \left(-\frac{7k^4}{4} + \frac{(-3 - 8c_0 + 2\lambda_2)k^2}{4} + \lambda_2 + \frac{5}{4}\right)A^2 + \left(-8k^4 + \frac{(32c_0 + 16\lambda_2)k^2}{4} - \lambda_2 - \frac{1}{2}\right)A_2.$

19

$\varepsilon^3 \psi_{10}$:

$$\frac{\mathrm{d}}{\mathrm{d}T}A = \left(\frac{5k^6}{2}+\frac{(1-8c_0-3\lambda_2)\,k^4}{2}+\frac{\left(\frac{7}{2}+12c_0+\lambda_2\right)k^2}{2}-\frac{27}{4}-3\lambda_2\right)A|A|^2+\left(\frac{(-4c_0-1)\,k^2}{2}+2\lambda_2+\frac{5}{2}\right)AA_0$$

$$+\left(4k^4+4\left(-\frac{3}{8}-\frac{5c_0}{2}-\frac{\lambda_2}{2}\right)k^2+4\left(\frac{5}{8}+\frac{\lambda_2}{2}\right)\right)\overline{A}A_2+\left(-k^2+1\right)\alpha_2 A.$$

From the area constraint we get the condition $0 = A_0 + k^2|A|^2$ for the ψ_{00} mode, which gives

$$\alpha_2 = \frac{1}{2}\left(k^4 - 8k^2 c_0 + 4\lambda_2 + 5\right)|A|^2 - \beta_2.$$

We used directly the ε scale of λ_2, hence we only get back the zero eigenvalue at $\varepsilon\psi_1$. The above equations at $\varepsilon^2\psi_{00}$ and $\varepsilon^2\psi_{20}$ give

$$A_0 = \frac{1}{2\lambda_2 + 1}\left(\left(k^4 + (-8c_0 - 2\lambda_2 - 1)\,k^2 + 4\lambda_2 + 5\right)|A|^2 + -2\alpha_2 - 2\beta_2\right), \quad \text{and} \tag{55}$$

$$A_2 = -\frac{A^2\left(7k^4 + (3 + 8c_0 - 2\lambda_2)\,k^2 - 4\lambda_2 - 5\right)}{2\left(16k^4 + (-16c_0 - 8\lambda_2)\,k^2 + 2\lambda_2 + 1\right).} \tag{56}$$

The dependence on β_2 here comes from the dependence of λ_1 on λ_2. Combining everything leads at $\varepsilon^3\psi_{10}$ to the solvability condition (54) with

$$a = k^2 - 1,$$

$$b = \frac{5}{(k^2-1)\,k^2\,(4k^4-5k^2+4c_0-1)}\left(\frac{3}{20}+k^{14}+\left(4c_0-\frac{73}{20}\right)k^{12}+\left(\frac{8c_0}{5}-\frac{13}{10}\right)k^{10}+\left(\frac{32}{5}c_0^2-\frac{52}{5}c_0+\frac{73}{20}\right)k^8\right.$$

$$\left.+\left(\frac{16}{5}c_0^2-8c_0+\frac{31}{5}\right)k^6+\left(\frac{4c_0}{5}-\frac{43}{20}\right)k^4+\left(\frac{12c_0}{5}-\frac{3}{2}\right)k^2\right).$$

Recall that here $k = k_m = 2m\pi/L$, hence $a < 0$ for $L > 2m\pi$, and similarly $b < 0$ for non small L. For instance, $a \approx -0.6$ and $b \approx -3$ in Fig.5, where we compare the AE predictions for $m = 1$ pearling with $c_0 = 0$ and $L = 10$ with numerics. In any case for $ab > 0$ we set $\beta_2 = -1$ (subcritical case), and otherwise $\beta_2 = 1$ (supercritical case), giving the amplitude $A = \sqrt{\left|\frac{a}{b}\right|}$, with also α_2 uniquely determined. The change of the volume can be approximated by inserting the amplitude Ansatz, giving $0 = A_0 + A^2 + \beta_2$ at $\varepsilon^2\psi_{00}$, and comparison with (55) shows that preserving the area and the volume is not possible along the pearling branch.

4.2.2 Wrinkling instability

For the primary wrinkling instability at $\lambda_2(0,2) = 3/2$ we have the ansatz

$$\varepsilon\,u(\varphi) = \varepsilon A e^{2\mathrm{i}\varphi} + \varepsilon^2\left(\frac{1}{2}A_0 + A_4 e^{4\mathrm{i}\varphi}\right) + \text{c.c.} + \mathcal{O}(\varepsilon^3),$$

again with $\varepsilon = \sqrt{\frac{|\lambda_2 - \lambda_2^{(0,2)}|}{\beta_2}}$ and $A = A(T)$, $T = \varepsilon^2 t$, and obtain the following.

$\varepsilon\psi_{02}$: $0 = 3A\left(\lambda_2 - \frac{3}{2}\right).$

$\varepsilon^2 \psi_{00}$: $0 = \frac{1}{4} (-40\lambda_2 + 82) |A|^2 - \left(\lambda_2 + \frac{1}{2}\right) A_0 - \beta_2 - \alpha_2.$

$\varepsilon^2 \psi_{04}$: $0 = \left(-9\lambda_2 + \frac{369}{4}\right) A^2 + \left(15\lambda_2 - \frac{225}{2}\right) A_4.$

$\varepsilon^3 \psi_{02}$: $\frac{d}{dT} A = -6 \left(\lambda_2 - \frac{11}{4}\right) AA_0 + \frac{1}{4} (-120\lambda_2 + 1170) \overline{A}A_4 - 3A\alpha_2 - 3 \left(-\lambda_2 + \frac{221}{4}\right) |A|^2 A.$

From the area constraint at $\varepsilon^2 \psi_{00}$ we have $0 = 8|A|^2 + 2A_0$, leading to $\alpha_2 = \frac{3(15-4\lambda_2)|A|^2}{2} - \beta_2$. Thus $\lambda_2^{(0,2)} = \frac{3}{2}$, $A_0 = \frac{11}{4}|A|^2 - \frac{\beta_2}{2} - \frac{\alpha_2}{2}$, $A_4 = \frac{7}{8}A^2$ and finally $\alpha_2 = \frac{27}{2}|A|^2 - \beta_2$. This ultimately leads to the solvability condition

$$\frac{d}{dT} A = (3\beta_2 - 15.19|A|^2)A, \tag{57}$$

which is notably independent of c_0 and L, and yields supercritical wrinkling bifurcations for $\beta_2 = 1$.

4.2.3 Coiling/buckling instability

For the instability with critical wave vector $(m, n) = (1, 1)$ and $(m, n) = (1, -1)$ we choose the ansatz

$$\varepsilon u(x, \varphi) = \varepsilon (A\psi_{11} + B\psi_{1-1}) + \varepsilon^2 \left(\frac{1}{2}A_{00} + A_{22}\psi_{22} + B_{22}\psi_{2-2} + A_{20}\psi_{20} + A_{02}\psi_{02}\right) + \text{c.c.} + \mathcal{O}(\varepsilon^3), \tag{58}$$

with $\varepsilon = \sqrt{\frac{|\lambda_2 - \lambda_2^{mm}|}{\beta_2}}$ and $T = \varepsilon^2 t$. Using the amplitude formalism, this gives a cubic *system* of reduced equations for A, B, which by $O(2) \times O(2)$ symmetry must read

$$\frac{d}{dT} A = A(a\beta_2 + b_1|A|^2 + b_2|B|^2), \tag{59a}$$

$$\frac{d}{dT} B = B(a\beta_2 + b_2|A|^2 + b_1|B|^2). \tag{59b}$$

From that we can directly recover the two types of solutions: Buckling with $A = \sqrt{\left|\frac{a}{b_1}\right|}$ and $B = 0$

or the other way round; coiling with $A = B = \pm\sqrt{\left|\frac{a}{b_1 + b_2}\right|}$. Here again $\beta_2 = \pm 1$, depending on the signs of a, b_1, and $b_1 + b_2$.

We have $a = k_m^2$, but the computation of the coefficients b_1 and b_2 naturally is more cumbersome than for the scalar case (pearling and wrinkling), and therefore relegated to Appendix A.1. Here we instead briefly comment on the bifurcation directions, and stability of the bifurcating branches under volume and area preserving flows, see also Fig.3. The Jacobian of the rhs of (59) at a steady state (A, B) is

$$\begin{pmatrix} a + 3b_1 A^2 + b_2 B^2 & 2b_2 AB \\ 2b_2 AB & a + b_2 A^2 + 3b_1 B^2 \end{pmatrix}.$$

For $a > 0$, on the coil solution branch the eigenvalues are $\sigma_1 = (a\beta_2 + 3\text{sign}(b_1)|a\beta_2|)$ and $\sigma_2 = (a\beta_2 + \frac{b_2}{|b_1|}|a\beta_2|)$. Hence the coils are stable for $\frac{b_2}{|b_1|} < -\text{sign}(\beta_2)$.

For the buckling the Jacobian has the eigenvalues

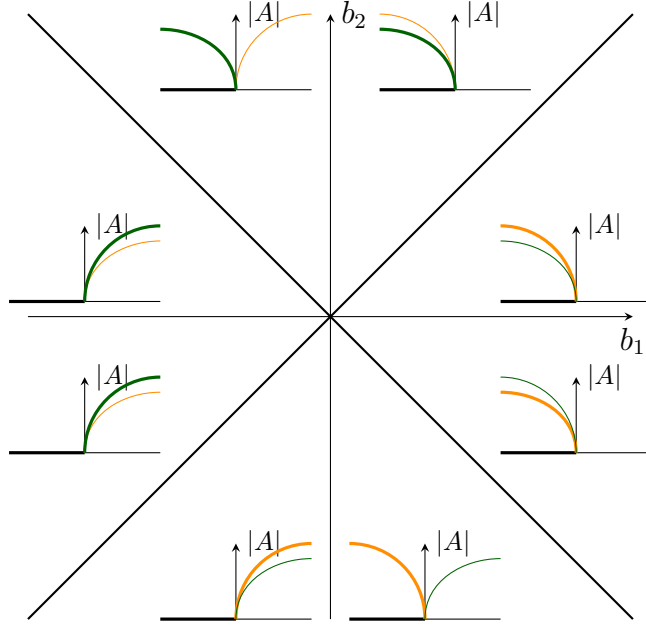$$\sigma_1 = 2\frac{b_2 + b_1}{|b_1 + b_2|} \qquad \sigma_2 = \frac{b_2 - b_1}{|b_1 + b_2|},$$

Figure 3: Schematic linearized stability diagram of the amplitude equation depending on b_1 and b_2. Orange stands for the coil and green for the wave branch. Thick lines indicate stable solutions.

where σ_1 corresponds to the eigenvector $v_1 = (1,1)^T$ and σ_2 to $v_2 = (1,-1)^T$. Hence the relevant eigenvalue is σ_2, which is negative for $b_2 < b_1$. In §5 we give two comparisons of the predictions from (59) with numerics, namely c_0 and $L = 10$ yielding $(a, b_1, b_2) \approx (0.39, -0.67, -0.82)$ in Fig.4, and $c_0 = 0.48$ and $L = 10$ yielding $(a, b_1, b_2) = (0.39, -0.083, 0.56)$ in Fig.9. In both cases we get the correct branching and stability predictions, and also very good quantitative agreement.

5   Numerical examples

We now use numerical continuation and bifurcation methods to corroborate the local results from §4, and to extend them to a more global picture. This includes the study of secondary bifurcations with interesting stable shapes far away from the cylinder. The numerical setup follows the stability analysis in §3.3 and §4.2. Namely, we throughout fix the period L, and the area $\mathcal{A} = \mathcal{A}(X)$, and initially use λ_2 as the primary bifurcation parameter and λ_1 and $\mathcal{V}(X)$ as secondary (dependent) parameters. The linearized stability of the solutions, however, is then computed for fixed $\mathcal{A}(X)$ and $\mathcal{V}(X)$ while λ_1 and λ_2 are free parameters. Due to the radius-length scaling invariance of the Helfrich energy (1) and the area and volume constraint in the dynamical problem, it is useful to introduce the reduced volume

$$v = \mathcal{V}(X)/\mathcal{V}_0, \tag{60}$$

where $\mathcal{V}_0$ is the volume of the straight cylinder with the same $\mathcal{A}(X)$, compare [JSL93], and we normalize the energy

$$\tilde{E}(X) = \frac{1}{\mathcal{A}} \int_X (H - c_0)^2 \, \mathrm{d}S. \tag{61}$$

Also for our numerics we focus on the three exemplary cases

$$\text{(a) } c_0 = 0, \quad \text{(b) } c_0 = -1, \quad \text{and (c) } c_0 = 0.48$$

from Fig.2, and mostly we use $L = 10$. For (a) and (b) this is no significant restriction as in these cases the primary bifurcations (to pearling, buckling and coiling in (a), and to pearling and wrinkling

in (b)) are of long wave type for any (sufficiently large) L, i.e., a different L gives the same types of primary bifurcations with different axial (maximal) periods L (and the wrinkling is independent of L). However, for (c) and sufficiently large L (preferably an integer multiple of the critical period $\ell \approx 7.5$) we have a finite wave number pearling instability. Thus, besides the case $L=10$ (for comparison with (a) and (b)), for (c) we shall consider different multiples of 7.5 for L, namely $L=15, L=30$, and $L=45$, allowing 2, 4, and 6, pearls on the primary branch. The influence of L will then be the behavior of this branch away from bifurcation, which loses stability in a bifurcation to a single pearl branch, and this BP moves closer to the primary BP with increasing L. This is further discussed in §6.

In the numerics we (as always) have to find a compromise between speed and accuracy. For the default $L = 10$ we start with an initial discretization of the straight cylinder $\mathcal{C}_L$ by $n_p \approx 3000$ mesh points; the continuation of the nontrivial branches then often requires mesh refinement (and coarsening), typically leading to meshes of 4000 to 5000 points. For the longer cylinders for $c_0 = 0.48$ we increase this to up to 12000 mesh points. A simple measure of numerical resolution is the comparison of the λ_2 values of the numerical BPs from $\mathcal{C}_L$ with their analytical values from §3.1, and here we note that in all cases we have agreement of at least 4 digits. Moreover, we also compare some numerical nontrivial branches with their descriptions by the AEs, and find excellent agreement.

Remark 5.1. Some cylindrical solutions have similarities with axisymmetric closed vesicle solutions of (4). We recall from [JSL93] or [MU24b], that from the sphere the first bifurcation is to prolates (rods) and oblates (wafers). For mildly negative or positive c_0 the prolates are stable near bifurcation and the oblates unstable, and continuing the prolates they become dumbbells (two balls connected by a thin neck), from which pea shaped vesicles bifurcate which become stable as one of the ball shrinks. For sufficiently negative c_0, the oblates are stable near bifurcation, and continuing the branch they become discocytes of biconcave red blood cell shape. Here we see some reminiscent behavior, e.g., secondary bifurcations of stable wrinkles with "embedded biconcave shapes" for sufficiently negative c_0, see, e.g., Fig.7E, and secondary bifurcations to "unequal pearls" from the pearling at positive c_0 (see Figures 10–12). ⌋

We complement our results by some (area and volume conserving) numerical flows close to steady states, and for these perturb steady states X_0 in two different ways: one is

$$\tilde{X}_0 = X_0 + \delta u_0 N_0, \quad u_0 = \frac{1}{1 + \xi x^2} \cos(\varphi), \tag{62}$$

where x is the coordinate along the cylinder axis, and φ the polar angle orthogonal to it, and $\delta \in \mathbb{R}$ and $\xi > 0$ are parameters, with typically $\xi = 1$ and $\delta = -0.125$ or $\delta = -0.25$ (recall that N is the inner normal). The other way is

$$\tilde{X}_0 = X_0 + \delta u_0 N_0, \qquad \text{with } u_0 = \psi_{\text{crit}}, \tag{63}$$

where ψ_{crit} is (the u component of) the eigenvector to the largest eigenvalue of the Jacobian at X_0, and typically $\delta = -0.5$. Due to the negative δ combined with the inner normal N, perturbations of type (62) in general induce a small increase of the initial volume $\mathcal{V}_0 = \mathcal{V} + \mathcal{V}_\delta$ and area $\mathcal{A}_0 = \mathcal{A} + \mathcal{A}_\delta$, which are conserved under the flow. On the other hand, perturbations of type (63) are area and volume preserving to linear order.

Our numerical flows $t \mapsto (X(t), \Lambda(t)) = \Psi_{\text{num}}(t; h)X_0$ are *ad hoc* approximations with a time step-size h and tolerance `tol` (see Appendix A.2), and we summarize the results from our flow experiments as follows:

1. Linearly stable X_0 (at $(\mathcal{V}, \mathcal{A})$) are also stable under the flow at the perturbed $(\mathcal{V}_0, \mathcal{A}_0)$, and the solution flows back to the respective type (pearling, coiling, ...) at $(\mathcal{V}_0, \mathcal{A}_0)$, with a small change in (λ_1, λ_2). See, e.g., Fig.6(a,b).

2. If X_0 at $(\mathcal{V}, \mathcal{A})$ is linearly unstable, then we generally expect $X(t)$ to flow to the nearest stable steady state (of in general a different class), see Fig.6(c_2). However, if we have a significant perturbation of $(\mathcal{A}_0, \mathcal{V}_0)$, then $X(t)$ may still flow to a similar steady state close to X_0 by adapting (λ_1, λ_2), see, e.g., Fig.6(c_1). This underlines the fact that $\lambda_{1,2}$ are dynamical variables.
3. Naturally, we want E to decrease monotonously in t, cf.(6), which if violated gives an easy indicator of poor numerics. The monotonous decrease of E often requires rather small stepsizes and tolerances, and a result is that in many examples a single numerical flow to steady state is as expensive as the computation of the full BD of steady states, which we take as a strong argument for our steady state continuation and bifurcation approach.

5.1 $c_0 = 0$

For $L = 10$ and $c_0 = 0$, Corollary 3.7 gives that the cylinder destabilizes at $\lambda_2 \approx -0.95$ to pearling, $(m, n) = (1, 0)$, and at $\lambda_2 \approx 1.19$ to modes $(m, n) = (1, 1)$. Figure 4 shows the BDs and samples starting in (a_1) with the energy E over the reduced volume v. Here all branches bifurcate from
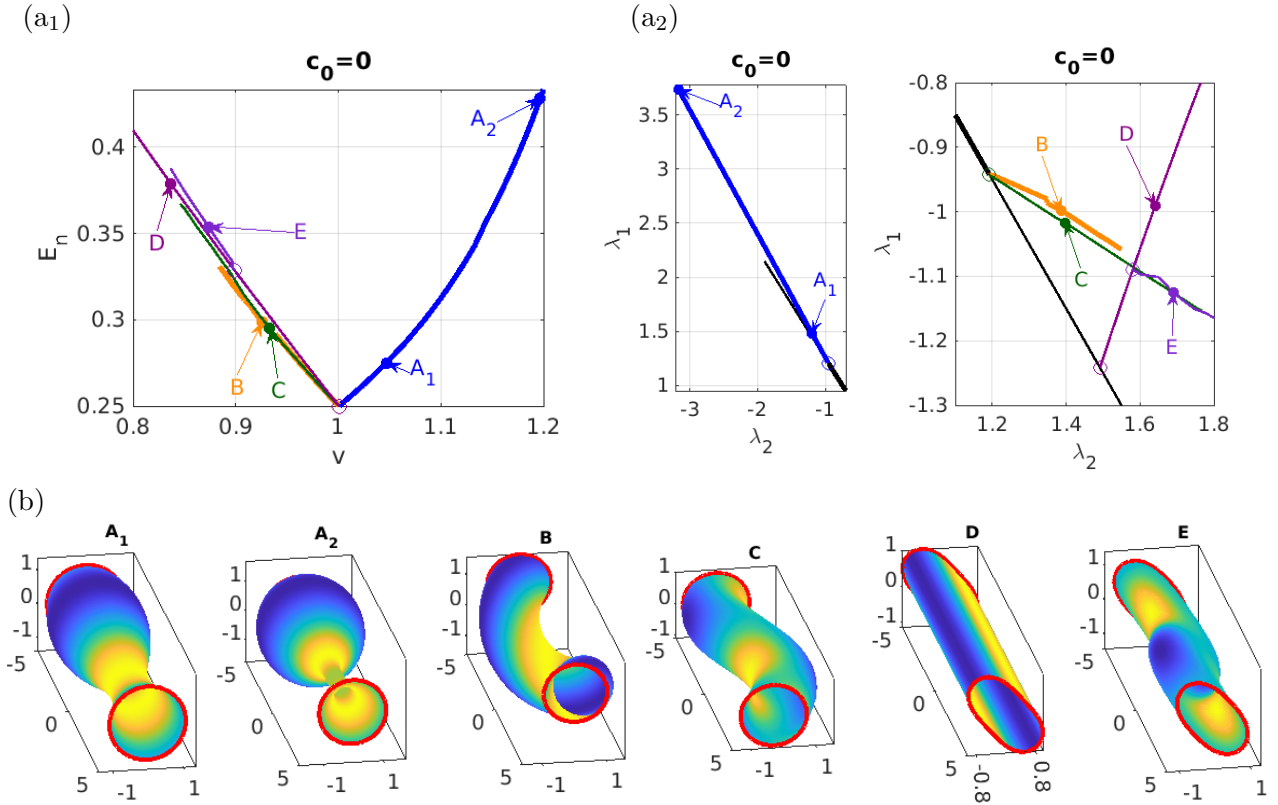

Figure 4: Basic BD for $c_0 = 0$, $L = 10$. (a_1) Energy E over reduced volume v. The family of cylinders $\mathcal{C}_{10}$ parameterized by λ_1 corresponds to the point where all primary branches bifurcate; A=pearls, B=coils, C=buckling, D=wrinkling; E is a secondary bifurcation from D, yielding a mix of buckling and wrinkling. (a_2) Relations between λ_1 and λ_2. The cylinders are the black branch, stable for $\lambda_2 \in (-0.95, 1.19)$. Bifurcation of A at $\lambda_2 \approx -0.95$, bifurcation of B,C at $\lambda_2 \approx 1.19$, and bifurcation of D at $\lambda_2 = 3/2$. Samples in (b); here the colors indicate u from the current continuation step, with blue for $u < 0$ (yellow for $u > 0$) indicating that X moves outward (inward) along the branch. The periodic boundaries are shown in red for better visibility.

$v = 1$, but (a_2) shows that they are well separated in the (λ_1, λ_2) plane. As stated in §4.2.1, the blue pearling branch starts stable close to the bifurcation point (sample A_1), and stays stable up to rather strong deformations of the original cylinder, sample A_2. The area constraint prevents the branch from growing to arbitrary volumes, but due to neck development the continuation becomes more difficult

24

for larger v. From the mode $(m,n) = (1,1)$ at $\lambda_2 \approx 1.19$ we find buckling and coiling. The coefficients in (59) are $(a, b_1, b_2) = (0.39, -0.4, -0.67)$, and as predicted (see Remark 5.2) the coiling (sample B) is stable close to bifurcation, while the buckling (sample C) is unstable. This behavior continues to small v, with no secondary bifurcations.

Additionally we show one wrinkling branch (sample D) as a later bifurcation from the cylinder, and a secondary bifurcation to a wrinkling–buckling mix (sample E). However, these solutions are all linearly unstable in the $\lambda_{1,2}$ range shown, at the given $\mathcal{V}$ and $\mathcal{A}$.
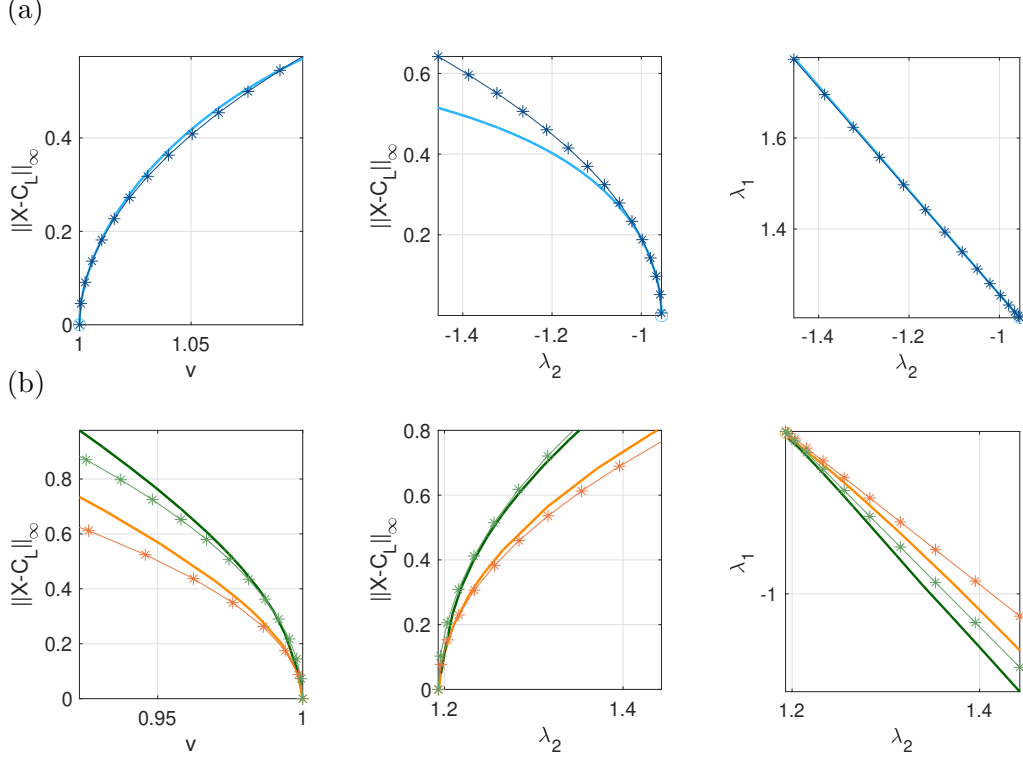

Figure 5: $c_0 = 0$, comparison of numerics and AE predictions (lines with *), (a) pearling, (b) coils (orange) and buckling (green). Left and center: Amplitude over reduced volume v, and over λ_2. Right: λ_1 over λ_2).

Remark 5.2. The amplitude formalism in §4.2 is only expected to be valid in a small neighborhood of the bifurcation points. In Fig. 5 we show comparisons between the numerical computations and the AE predictions. Here the amplitude formalism for the pearling

$$u = \varepsilon A \psi_{10} + \mathcal{O}(\varepsilon^2), \quad \lambda_2 = \lambda_2(1,0) - \varepsilon^2, \quad \lambda_1 = \lambda_1(1,0) + \alpha_2 \varepsilon^2 + \mathcal{O}(\varepsilon^4),$$

yields $\dfrac{\mathrm{d}}{\mathrm{d}T} A = A(0.61 - 2.96 A^2)$ and $\alpha_2 = 0.66 A^2 - 1$, and that for the wrinkling $u = \varepsilon A \psi_{01} + \mathcal{O}(\varepsilon^2)$, $\lambda_2 = \lambda_2(0,1) + \varepsilon^2$, $\lambda_1 = \lambda_1(0,1) + \alpha_2 \varepsilon^2 + \mathcal{O}(\varepsilon^4)$ yields the universal AE (57), i.e., $\dfrac{\mathrm{d}}{\mathrm{d}T} A = A(3 - 15.19 A^2)$ and $\alpha_2 = \frac{27}{2} A^2 - 1$. For both, pearling and wrinkling, we find an excellent match with the numerics. ⌋

In Fig.6 we show numerical flows from the steady states A–C from Fig.4, perturbed according to (62), with parameters given in Table 1. In all cases we integrate until $\|\partial_t u\|_\infty < 0.001$. The plots on the left show the initially perturbed X_0, and X at the end of the DNS colored by the last update δu, such that $u_t \approx \delta u / h$, where h is the current stepsize. The plots on the right show the evolution of $E(t)$ and $\lambda_{1,2}$, and the relative errors in $\mathcal{A}$ and $\mathcal{V}$ (with the error in $\mathcal{V}$ always two orders of magnitude larger than that in $\mathcal{A}$).
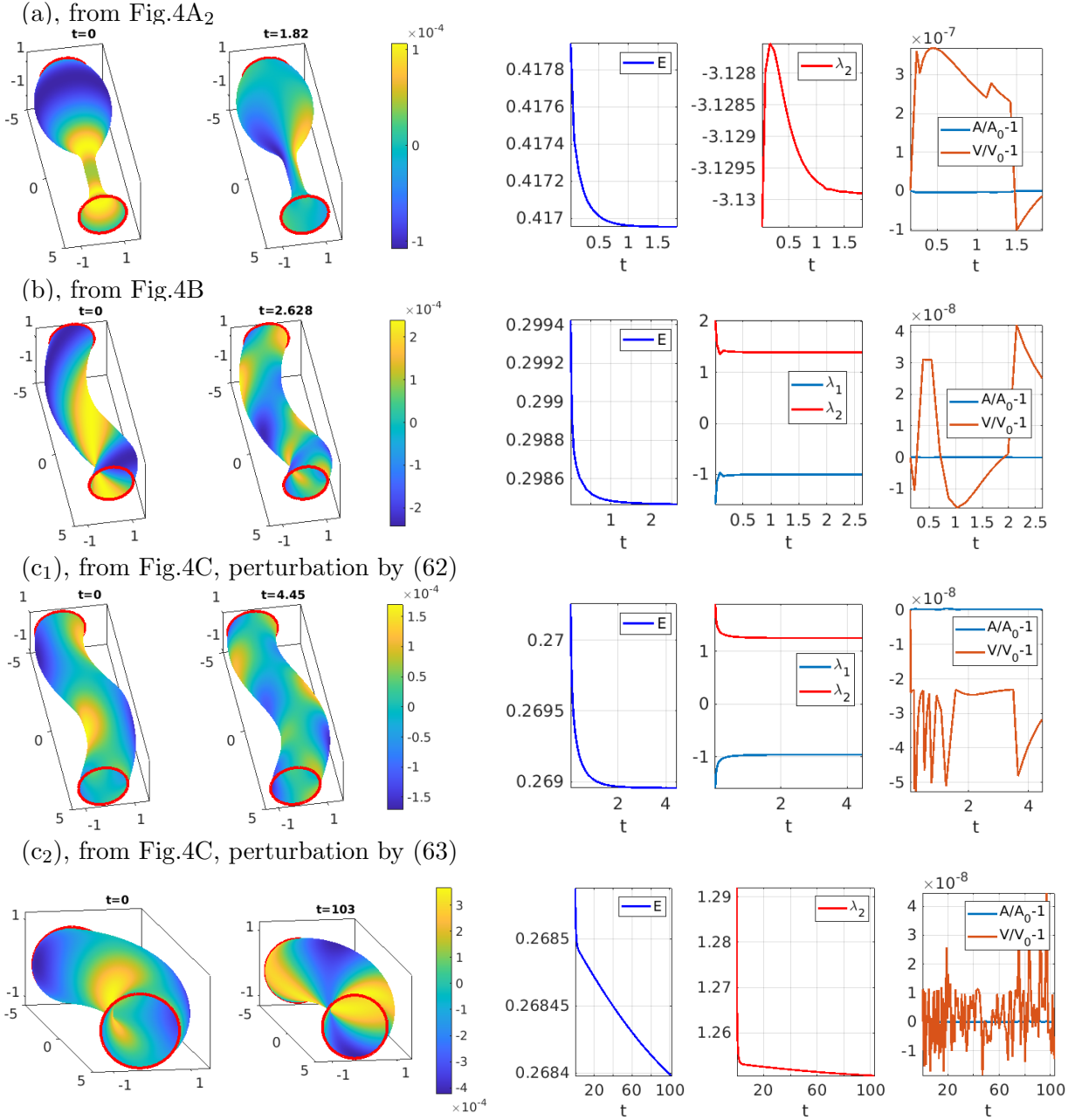
Figure 6: Numerical flows from perturbations of states from Fig.4; initial and 'final' state, and evolution of E, $\lambda_{1,2}$ (only λ_2 in (a) and (c$_2$)), and deviations from intial area and volume; very slow evolution in (c$_2$).

The first two flows start near stable steady states $(X_0, \lambda_{1,0}, \lambda_{2,0})$, and as expected flow back to near X_0 rather quickly, with partly significant changes of (λ_1, λ_2). However, the third flow (c$_1$) is somewhat surprising. State C from Fig.4 is linearly unstable, but the perturbed X_0 flows to another buckling by adjusting $\lambda_{1,2}$ at the increased area and volume, where this buckling is stable. On the other hand, in (c$_2$) for the (linearly) area and volume preserving initial perturbation into the most unstable direction (which point towards coils), the behavior is different: The solution now converges to a coil, with a rather small flow throughout; λ_1 hardly changes at all, λ_2 only very slightly, and the convergence is very slow (since the leading eigenvalue of the target coil is negative but very close to zero). For all flows, we can use the final state as an initial guess for steady state continuation (e.g., in λ_2), and the obtained numerical steady states then are (volume preserving) linearly stable.

26

Table 1: Spectral data (n_{unst}=number of (V-preserving) unstable directions, μ_{crit}=least stable/most unstable eigenvalue), perturbation parameter δ (ξ=1 throughout), and results for DNS in Fig.6; $A_0=20\pi, V_0=10\pi$. Initial perturbations for A–C of type (62), and for C* of type (63). $(\lambda_1, \lambda_2)_0$ are the values at the (perturbed) steady state.

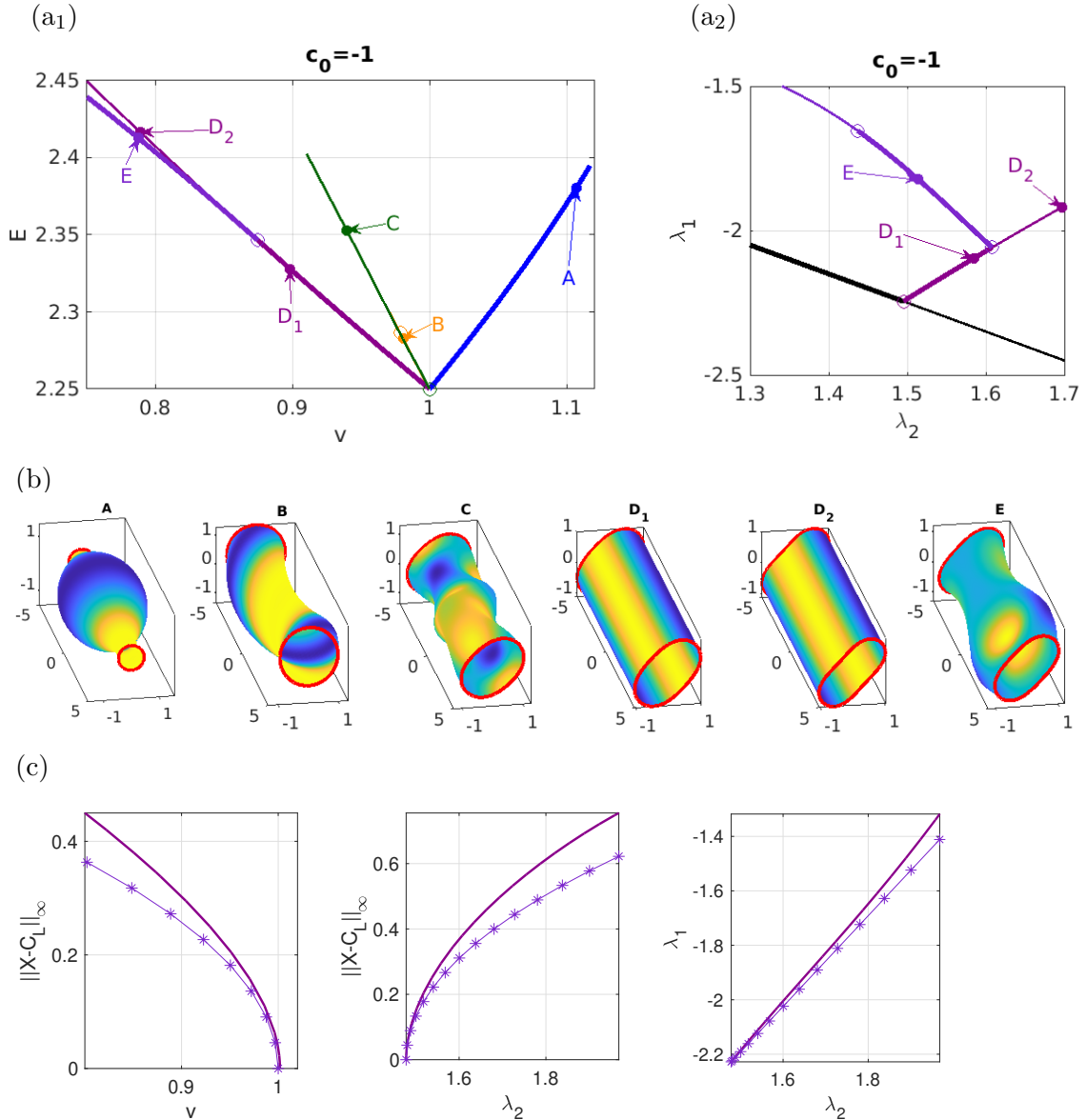| IC type	A_2 (pearling)	B (coiling)	C (buckling)	C (buckling)*
$n_{\mathrm{unst}}, \mu_{\mathrm{crit}}$	0, -2.22	0, -0.018	1, 0.012	1, 0.012
δ	-0.125	-0.25	-0.25	0.5
$(A - A_0)/A_0$	0.0012	0.0003	0.0125	0.0024
$(V - V_0)/V_0$	0.0011	0.0004	0.02	0.004
$(\lambda_1, \lambda_2)_0$	(3.734, -3.165)	(-0.999, 1.387)	(-0.972, 1.29)	(-0.972, 1.29)
$(\lambda_1, \lambda_2)_{\mathrm{end}}$	(3.701, -3.133)	(-0.999, 1.389)	(-1.003, 1.367)	(-0.965, 1.25)

Figure 7: Basic BD (a) for $c_0 = -1$, $L = 10$, and samples (b). (a_1) Energy E over v; (a_2) λ_1 over λ_2 for the wrinkling D and 'embedded oblates' E. (c) Comparison with AE prediction for primary wrinkling.

5.2 $c_0 = -1$

For (strongly) negative c_0, the wrinkling branches and their secondary bifurcations become relevant. Fig.7(a,b) shows basic results for $c_0 = -1$ and $L=10$, and (c) a comparison with the AE predictions from (57) for wrinkling, again with very good agreement, cf. Remark 5.2. As before, at negative $\lambda_2 \approx -2.254$ and $\lambda_1 \approx 1.5$ (cf.Fig.2), $\mathcal{C}_r$ looses stability to pearling, but now at positive $\lambda_2 = 3/2$ and $\lambda_1 = -9/4$ it looses stability to the wrinkling branch (samples $D_{1,2}$), while the bifurcation to buckling and coiling is at a later $(\lambda_1, \lambda_2) \approx (-3.77, 3.021)$ and yields initially unstable branches. The wrinkling is initially stable, but at $\lambda_2 \approx 1.6$ loose stability to "oblates embedded in wrinkling", see sample E, and Remark 5.1.

Figure 8 shows some numerical flows from states from Fig.7, focusing on wrinkling perturbed according to (62) (pearling is again stable, also under rather large perturbations). D_2 at its given $(\mathcal{A}_0, \mathcal{V}_0)$ is linearly (weakly) unstable, and the perturbation yields a slow evolution to an oblate wrinkling, with a very small change in E. In (b) and (c) we perturb a coiling and a buckling, and in both cases flow to wrinkling, and the bottom line of Fig.8 and similar experiments is that (stable) wrinkling and oblate wrinkling have rather large domains of attraction.

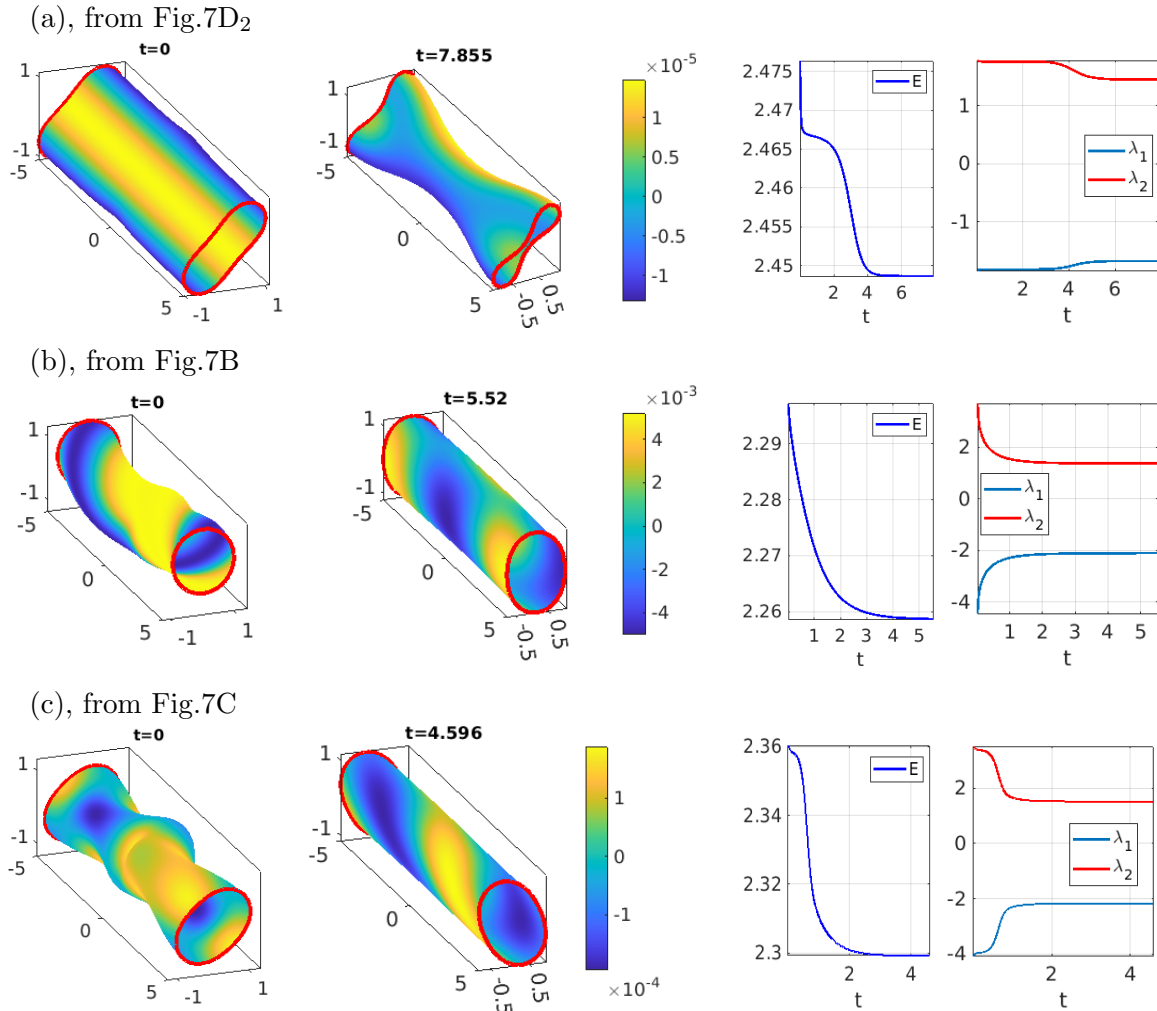(a), from Fig.7D_2

(b), from Fig.7B

(c), from Fig.7C

Figure 8: Numerical flows near states from Fig.7; initial perturbations of type (62) with $\delta = -0.25$. Flow to "embedded oblate", here at the boundary, in (a), and to wrinkling in (b,c).

5.3 $c_0 = 0.48$

Lastly, we consider positive c_0, specifically $c_0 = 0.48$. By Corollary 3.7, the cylinder destabilizes in a *finite wave length* pearling instability, and in a long wave instability to coiling and buckling. The finite pearling period is $\ell := \ell_p \approx 7.5$, and thus we will be mostly interested in length L as multiples of 7.5.

However, for comparison with the cases $c_0 = 0$ and $c_0 = -1$ we first again choose $L = 10$, and in Fig.9 give the BD of buckling and coils. The coefficients for the AE description (59) now are $(a, b_1, b_2) = (0.39, -0.083, 0.56)$, and in agreement with Fig.3 the buckling are now stable at bifurcation and the coils unstable. Moreover, we find interesting 2ndary bifurcations on both branches, where the buckling looses (coiling gains) stability, and these two BPs are connected by a stable intermediate branch, see sample C. The comparison with the AEs in (c) again shows the agreement close to bifurcation, but naturally the (cubic order) AEs cannot capture the fold of the coiling in λ_2.
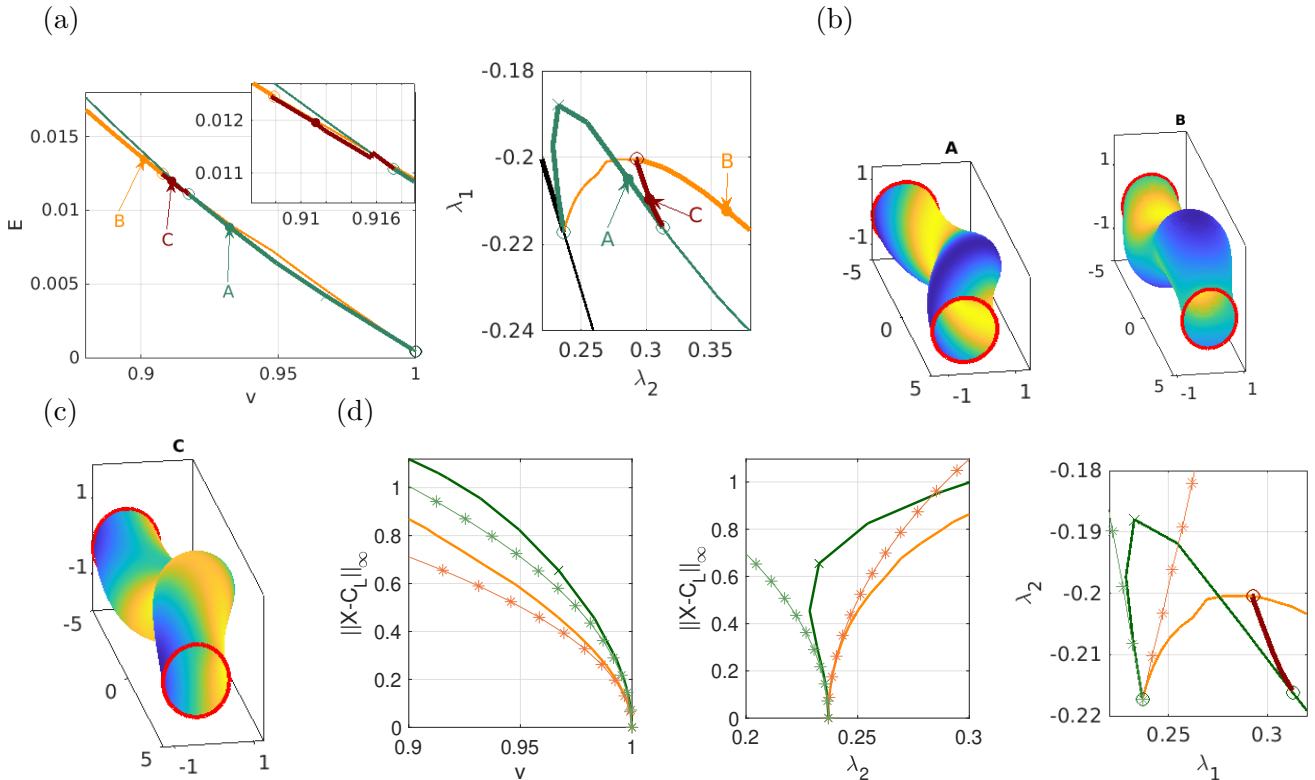

Figure 9: $c_0 = 0.48$, $L = 10$. Numerical BDs and samples in (a,b,c), where C shows a stable connection between the stable regimes of coiling and buckling. Comparison to AE predictions in (d).

Figure 10 shows the BD and samples for $L = 15$. To the right of $v = 1$ bifurcates the $m = 2$ pearling branch (at $\lambda_2 \approx -0.243$), and is initially stable (sample A_1). However, shortly after ($\lambda_2 \approx -0.3756$) there is a secondary bifurcation to a stable branch with double the period, sample B. On the other hand, the primary $m = 1$ pearling branch, sample C, (bifurcating at $\lambda_2 \approx -0.421$) is unstable throughout. The $(m, n) = (1, 1)$ coiling (sample D) and buckling (sample E) bifurcate at $\lambda_2 \approx 0.138$, and again the coiling is stable, and stays stable to rather small v, while the buckling is unstable. Wrinkling does not occur in the parameter regime considered; however, the (compared to $L = 10$ before) slightly larger $L = 15$ lets the pearling and coiling/buckling BPs move closer together, which is why we chose to present the $(m, n) = (2, 1)$ coiling F (unstable). Figure 11 shows the flow from a perturbation of A_2 to a B type solution but rather close to the BP. Therefore, the convergence to steady state is again very slow, as near bifurcation the stable B branch has a leading eigenvalue close to 0.
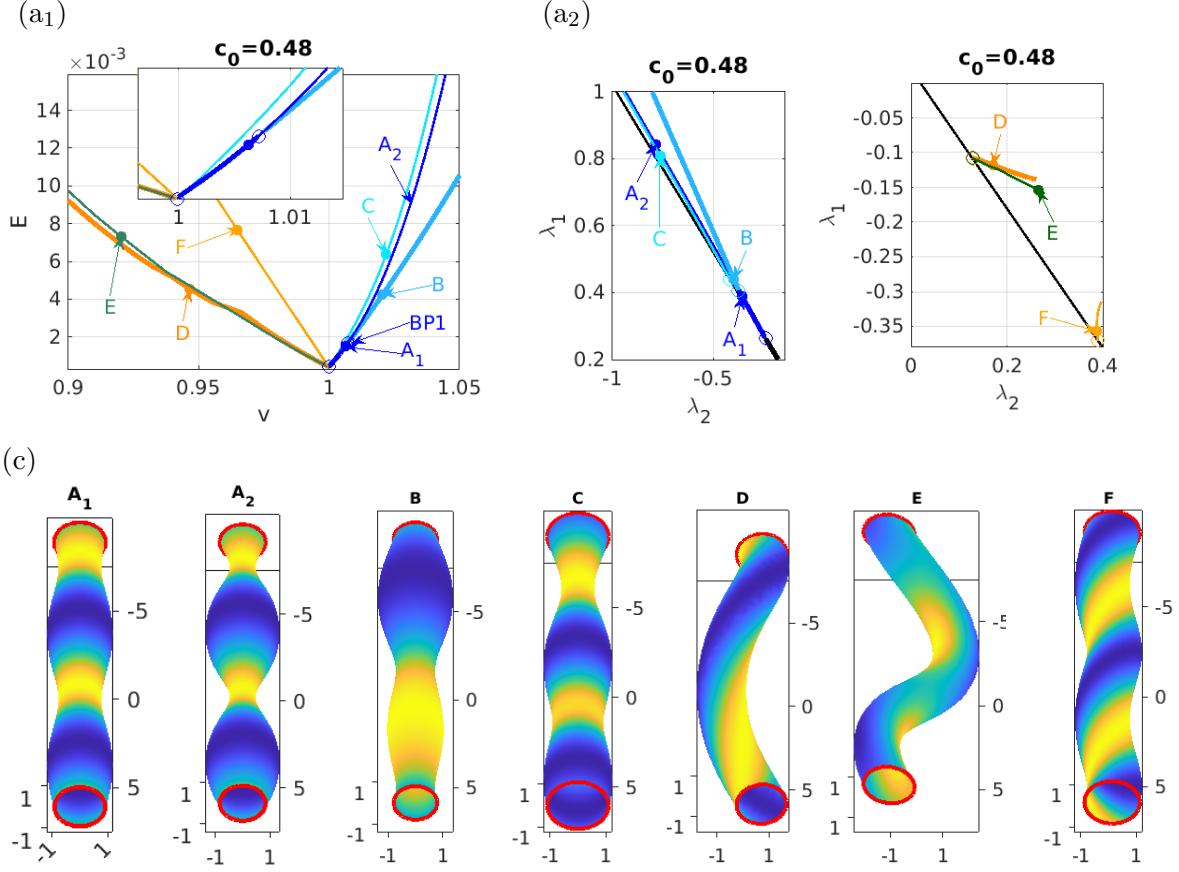
Figure 10: Basic BD for $c_0 = 0.48$, $L = 15$. (a) Energy E over reduced volume v, and λ_1 over λ_2. (b) Samples from primary pearling, A_1 stable, A_2 unstable. (c) further samples: B is period doubling from A branch, stable; C is the primary $m = 1$ pearling bifurcation, unstable; D is a (1,1)–coiling, stable; E is a (1,1)–buckling, unstable; F is a (2,1)–coiling.
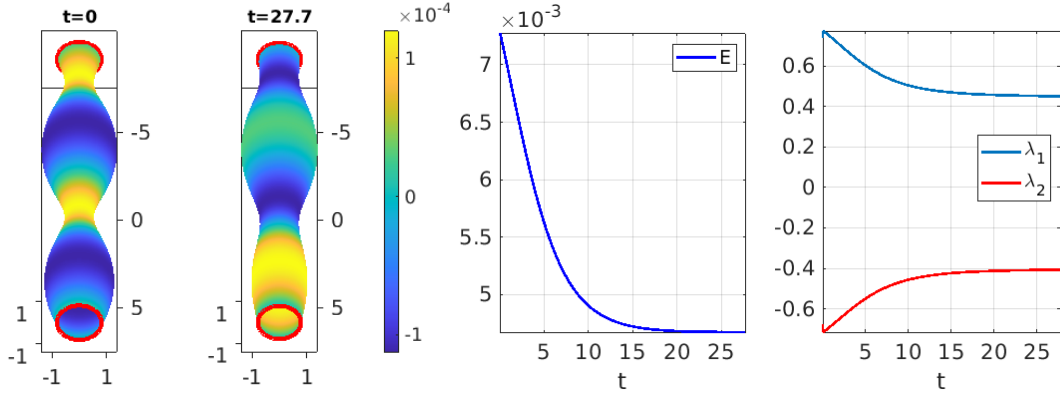
Figure 11: Sample flow from perturbation of A_2 of type (63) with $\delta = 0.5$, going to B type solution.

The main point of Fig.10 is that the choice of $c_0 = 0.48$ together with $L = 15$ yields the destabilization of the cylinder to the $m = 2$ pearling, but these solutions are only stable in a somewhat narrow range (in v, say). To further assess this, in Fig.12 we consider the primary pearling with $\ell = 7.5$ on twice the domain $L = 30$. The result shows that the range of stable $\ell = 7.5$ pearls shrinks with increasing L, and this continues for further increase of L, yielding the following dependence of

the reduced volume v_s of single pearling BPs from primary $\ell = 7.5$ pearling on L:

$$\begin{array}{c|cccc} L & 15 & 39 & 45 & 60 \\ \hline v_s & 1.0081 & 1.0063 & 1.0046 & 1.0035 \end{array} \tag{64}$$

We also ran some numerical flows from perturbations of A in Fig.12, and similarly at larger L, with results as in Fig.11, i.e., convergence to the single pearl solutions. However, these DNS are very expensive, partly due to the larger domain and hence larger scale discretization, but more importantly due to the very slow convergence of the flows.
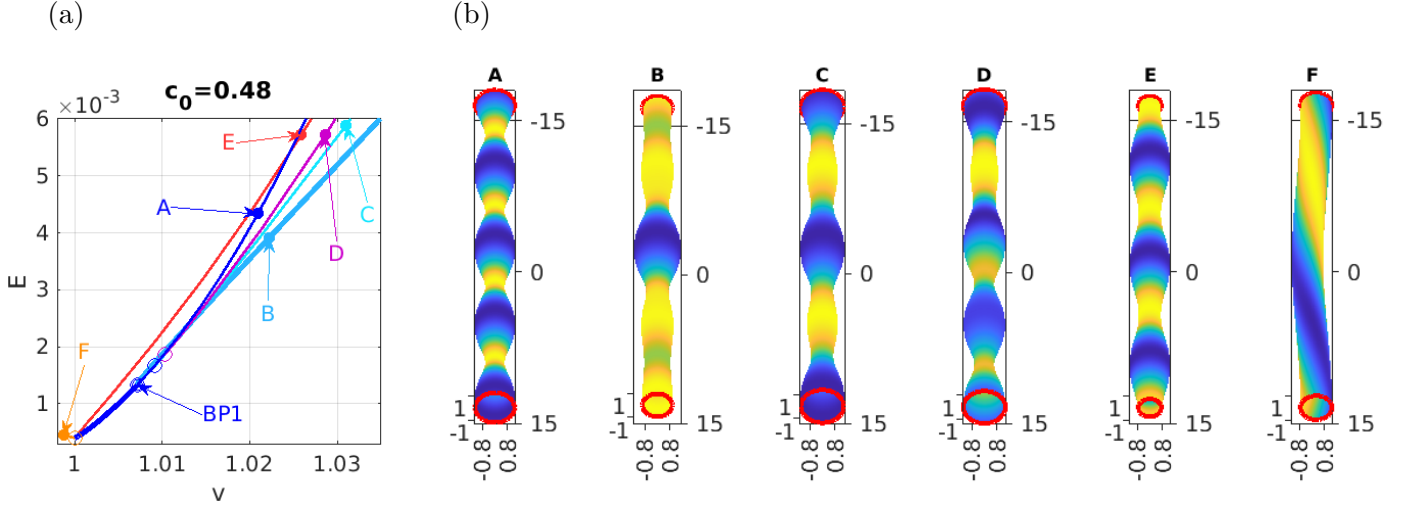
(a)   (b)

Figure 12: $c_0 = 0.48$, $L = 30$. The $m = 4$ (period $\ell = 7.5$) pearling A now looses stability at BP1 much closer to its primary bifurcation, to a single "localized" pearling branch, sample B. Further branches: C: $m = 2$ ($\ell = 15$) primary pearling; E: $m = 3$ ($\ell = 10$) primary pearling; D: 2ndary pearling from 2nd BP on $m = 1$ branch. F: primary $(m, n) = (1, 1)$ coiling.

6 Discussion and outlook

Motivated by experimental results as in Fig.1(a,b), we studied the bifurcations from straight cylinders $\mathcal{C}_L$ of lengths L (and wlog radius $r = 1$) in the Helfrich model (5). After showing well–posedness we discussed the linearization at $\mathcal{C}_L$ and derived the amplitude equations for the bifurcations of pearling, wrinkling, and coiling and buckling. Subsequently we used numerical continuation and bifurcation methods to extend the local bifurcations to a more global picture.

Our results initially suggest that (5) besides being very interesting mathematically is a possible model for the experiments in Fig.1(a,b). However, there also are strong discrepancies. One is that coiling (and buckling, which as far as we know is not clearly documented in experiments) always bifurcate with the maximum wavelength L allowed by the domain. For $c_0 > 0$, pearling can occur with a finite wavelength (Figs.10–12), but the stability range of finite wavelength pearling shrinks with increasing L, probably to zero for $L \to \infty$, which suggests that the experimental pearling as in Fig.1(a) cannot be described by (5).

Mathematically, the bifurcations of localized pearling from finite wave number pearling, with the pertinent BP moving closer to the primary bifurcation for larger domain size L, is similar to the bifurcation of localized patterns from periodic patterns in various dissipative systems, e.g., reaction diffusion (RD) systems or Swift–Hohenberg (SH) type equations. See, e.g., [BK07, HK09, BKL$^+$09, Kno15], and [Uec21, Chapters 8 and 9] for further references and numerics using `pde2path`. In these

systems, the localized patterns are usually attributed to subcritical primary bifurcations of periodic patterns, which are hence unstable, but stabilize after a fold at large amplitude. The localized patterns then show some "snaking" behavior with several folds in which the pattern grows, and with alternating stable and unstable segments of this snaking branch. Moreover, in the limit $L \to \infty$, the BP of the snaking branch converges to the primary BP of the periodic patterns.

The data in (64) for BP1 moving closer to $v = 1$ for larger L suggest a similar effect, but there are clear differences to the snaking scenario, and many open questions. In our numerics:

- After the loss of stability of the primary pearling A–branch, it never regains stability; in particular, we cannot find a fold (in v, say) for the A–branch.
- Similarly, we cannot find a fold or other loss of stability of the localized pearling B–branch.

The numerics here are harder for large L than for periodic and localized 1D (or 2D) patterns in, e.g., reaction diffusion systems, and for instance for $L = 60$ we only continue the A–branch and the B–branch to $v = 1.01$, such that these results are in some sense still local. Nevertheless, together with the fact that coiling and buckling is always of maximal wavelengths, they suggest that (5) may be a too simplistic model for experiments such as in Fig.1(a,b) (finite wavelength pearling and coiling).

For linearizations of (classical) dissipative systems on intervals $(0, L)$ at some steady state, the spectral gap between the critical eigenvalues and the rest of the spectrum shrinks as $L \to \infty$, and over $\mathbb{R}$ the amplitude equations (ODEs) for finite L must be replaced by modulation equations (PDEs) of Ginzburg–Landau type, incorporating the continuous curve of critical eigenvalues. See, e.g., [SU17, Part IV], and the references therein. For the Helfrich cylinders it is not clear how to proceed for $L \to \infty$. For long wave instabilities (buckling, coiling, wrinkling, and pearling except in a small range of positive c_0 as in Fig.10–12), without the volume constraint the critical curve $\mathbb{R} \ni k \mapsto \mu(k, n)$ is maximal at wave number $k = 0$, and we believe that instead of (5) a better way to incorporate the volume constraint is to consider the H^{-1} gradient flow for (1) with area constraint. This automatically conserves $\mathcal{V}$, and the critical curve is changed to $k \mapsto \tilde{\mu}(k, n) = k^2 \mu(k, n)$, such that we expect modulation equations with an (additional) conservation law; see, e.g., [ZS16, Hil20]. This, however, is beyond the scope of the current paper.

A Appendix

A.1 Buckling and coiling amplitude system computations

To derive the coefficients a, b_1, b_2 for the amplitude system (59) for the mixed mode instability we as usual plug the extended Ansatz (58) into (44) and sort wrt powers of ε.

$\varepsilon \psi_{11}$: $-\dfrac{1}{2} k^2 \left(k^2 - 4c_0 - 2\lambda_2 + 2 \right) A = 0.$

$\varepsilon \psi_{1-1}$: $-\dfrac{1}{2} k^2 \left(k^2 - 4c_0 - 2\lambda_2 + 2 \right) B = 0.$

$\varepsilon^2 \psi_{00}$:

$$0 = \left(-\frac{1}{2} + \frac{k^4}{2} + \frac{(5 - 8c_0 - 2\lambda_2) k^2}{2} - \lambda_2 \right) |A|^2 + \left(-\frac{1}{2} + \frac{k^4}{2} + \frac{(5 - 8c_0 - 2\lambda_2) k^2}{2} - \lambda_2 \right) |B|^2$$
$$- \lambda_2 A_{00} - \beta_2 - \alpha_2 - \frac{A_{00}}{2}.$$

$\varepsilon^2 \psi_{22}$: $0 = \left(-\dfrac{7k^4}{4} + \dfrac{(-8c_0 + 2\lambda_2 + 19) k^2}{4} - \dfrac{3\lambda_2}{2} + \dfrac{9}{4} \right) A^2 + \left(-8k^4 + \dfrac{(16\lambda_2 + 32c_0 - 64) k^2}{4} + 3\lambda_2 - \dfrac{9}{2} \right) A_{22}.$

$\varepsilon^2 \psi_{2-2}$: $0 = \left(-\dfrac{7k^4}{4} + \dfrac{(-8c_0 + 2\lambda_2 + 19) k^2}{4} - \dfrac{3\lambda_2}{2} + \dfrac{9}{4} \right) B^2 + \left(-8k^4 + \dfrac{(16\lambda_2 + 32c_0 - 64) k^2}{4} + 3\lambda_2 - \dfrac{9}{2} \right) B_{22}.$

$\varepsilon^2\psi_{20}$: $0 = \left(-\dfrac{7k^4}{2} + \dfrac{(2\lambda_2 + 8c_0 + 3)\,k^2}{2} - \lambda_2 - \dfrac{1}{2}\right)BA + \left(-8k^4 + \dfrac{(16c_0 + 8\lambda_2)\,k^2}{2} - \lambda_2 - \dfrac{1}{2}\right)A_{20}.$

$\varepsilon^2\psi_{02}$: $0 = 4A\left(\dfrac{k^4}{8} + \left(c_0 - \dfrac{\lambda_2}{4} + \dfrac{5}{8}\right)k^2 - \dfrac{3\lambda_2}{4} + \dfrac{9}{8}\right)\overline{B} + \left(3\lambda_2 - \dfrac{9}{2}\right)A_{02}.$

$\varepsilon^3\psi_{11}$:

$$\frac{\mathrm{d}}{\mathrm{d}T}A = \Bigg[\left(-k^2\alpha_2 - 4\left(-\frac{5k^6}{8} + \left(c_0 + \frac{3\lambda_2}{8} - 2\right)k^4 + \left(-\frac{c_0}{2} + \frac{5\lambda_2}{8} + \frac{23}{16}\right)k^2 - \frac{3\lambda_2}{4} + \frac{9}{8}\right)|A|^2\right.$$
$$\left.- 8\left(-\frac{5k^6}{8} + \left(c_0 + \frac{3\lambda_2}{8}\right)k^4 + \left(\frac{3c_0}{2} - \frac{3\lambda_2}{8} + \frac{15}{16}\right)k^2 - \frac{3\lambda_2}{4} + \frac{9}{8}\right)|B|^2 - 4k^2\left(\frac{1}{2}c_0 - \frac{3}{8}\right)A_{00}\right]A$$
$$+ 6\left(\left(c_0 + \frac{1}{4}\right)k^2 - \left(\lambda_2 - \frac{3}{2}\right)\right)A_{02}B - 10\left(-\frac{2k^4}{5} + \left(c_0 + \frac{\lambda_2}{5} - \frac{49}{20}\right)k^2 + \frac{3\lambda_2}{5} - \frac{9}{10}\right)A_{22}\overline{A}$$
$$- 2k^2\left(-2k^2 + c_0 + \lambda_2 - \frac{1}{4}\right)A_{02}\overline{B}.$$

$\varepsilon^3\psi_{1-1}$:

$$\frac{\mathrm{d}}{\mathrm{d}T}B = 6\left(\left(c_0 + \frac{1}{4}\right)k^2 - \lambda_2 + \frac{3}{2}\right)A\overline{A_{02}} + \left(-k^2\alpha_2 - 8\left(-\frac{5k^6}{8} + \left(c_0 + \frac{3\lambda_2}{8}\right)k^4 + \left(\frac{3c_0}{2} - \frac{3\lambda_2}{8} + \frac{15}{16}\right)k^2\right.\right.$$
$$\left.- \frac{3\lambda_2}{4} + \frac{9}{8}\right)|A|^2 - 4\left(-\frac{5k^6}{8} + \left(c_0 + \frac{3\lambda_2}{8} - 2\right)k^4 + \left(-\frac{c_0}{2} + \frac{5\lambda_2}{8} + \frac{23}{16}\right)k^2 - \frac{3\lambda_2}{4} + \frac{9}{8}\right)|B|^2$$
$$\left.- 2k^2\left(c_0 - \frac{3}{4}\right)A_{00}\right)B - 2k^2\left(-2k^2 + c_0 + \lambda_2 - \frac{1}{4}\right)A_{20}\overline{A} - 10\left(-\frac{2k^4}{5} + \left(c_0 + \frac{\lambda_2}{5} - \frac{49}{20}\right)k^2\right.$$
$$\left.+ \frac{3\lambda_2}{5} - \frac{9}{10}\right)B_{22}\overline{B}.$$

From the area constraint we get, at $\varepsilon^2\psi_{00}$, $0 = (k^2+1)|A|^2 + (k^2+1)|B|^2 + A_{00}$, and using $\lambda_2^{(1,1)} = \frac{1}{-k^2}\left(-\frac{1}{2}(k^2+1)^2 + (k^2+1) - (1 - 2\cdot c_0)\cdot k^2 - \frac{1}{2}\right)$ we solve the algebraic equations for the ε^2 modes:

$$A_{00} = -\frac{(4k^2c_0 - 2k^2 - 4c_0 + 3)}{k^2 - 4c_0 + 3}(|A|^2 + |B|^2) - \frac{2\alpha_2 + 2\beta_2}{k^2 - 4c_0 + 3},$$
$$A_{22} = -\frac{(2k^4 + 4k^2c_0 - 6k^2 - 4c_0 - 1)}{2(4k^4 + 7k^2 + 4c_0 + 1)}A^2, \quad B_{22} = -\frac{(2k^4 + 4k^2c_0 - 6k^2 - 4c_0 - 1)}{2(4k^4 + 7k^2 + 4c_0 + 1)}B^2,$$
$$A_{20} = -\frac{(6k^4 - 4k^2c_0 - 4k^2 - 4c_0 + 3)}{12k^4 - 7k^2 - 4c_0 + 3}AB, \quad A_{02} = -\frac{(4k^2c_0 + 4c_0 + 1)}{k^2 - 4c_0 - 1}A\overline{B}.$$

For the Lagrange multiplier expansion we get

$$\alpha_2 = \frac{k^2(k^2 - 8c_0 + 6)}{2}|A|^2 + \frac{k^2(k^2 - 8c_0 + 6)}{2}|B|^2 - \beta_2,$$

and altogether this gives the solvability condition (59) for A and B at ε^3 with

$$a = k^2,$$
$$b_1 = \frac{5}{4}k^6 + 5k^4c_0 + \frac{3}{4}k^4 + 9k^2c_0 - \frac{33}{4}k^2 - 6c_0 - \frac{3}{2}$$
$$+ \frac{3(2k^4 + 4k^2c_0 - 6k^2 - 4c_0 - 1)\left(-\frac{1}{2}k^4 + k^2c_0 - \frac{13}{4}k^2 - 2c_0 - \frac{1}{2}\right)}{4k^4 + 7k^2 + 4c_0 + 1},$$

$$b_2 = 3k^6 + 4k^4 c_0 - 6k^4 - 16k^2 c_0 - 3k^2 - 12c_0 - 3$$
$$+ \frac{6(4k^2 c_0 + 4c_0 + 1)\left(-\left(c_0 + \frac{1}{4}\right)k^2 + \frac{k^2}{2} - \frac{1}{2} - 2c_0\right)}{k^2 - 4c_0 - 1}$$
$$+ \frac{2(6k^4 - 4k^2 c_0 - 4k^2 - 4c_0 + 3)k^2\left(-\frac{3k^2}{2} - c_0 + \frac{3}{4}\right)}{12k^4 - 7k^2 - 4c_0 + 3}.$$

A.2 Numerical algorithms

The basic numerical setup for continuation in the differential geometric setting is explained in [MU24b], see also [pde25] for software download and demos. Here we recall some basic ideas[MU24b], and comment on some extensions. The numerics are based on finite element discrete differential geometry operators, as for instance implemented in `gptoolbox` [Jac24]. Let (X, `tri`) be a triangulation of the surface X with node coordinates $\mathbf{X}_j \in \mathbb{R}^{1 \times 3}$, $j \in \{1, \ldots, n_p\}$ and triangle list `tri`$\in \mathbb{R}^{n_t \times 3}$. Using linear hat functions $\phi_i : X \to \mathbb{R}$ with $\phi_i(\mathbf{X}_j) = \delta_{ij}$ with $i \in \{1, \ldots, n_p\}$, the operator (cotangent Laplacian)

$$L_{kl} = \int_X \nabla \phi_k \nabla \phi_l \, \mathrm{d}S = -\frac{1}{2}(\cot \alpha_{kl} + \cot \beta_{kl}). \tag{65}$$

approximates the (positive definite) Laplace–Beltrami operator, while for the FEM mass matrix M we use the so–called Voronoi mass matrix. Then, e.g., $MH(X) = \frac{1}{2}\langle LX, N \rangle$, where the vertex normals N are obtained from interpolating the normals of the adjacent triangles. For the Gaussian curvature K we use a discrete version of Gauss–Bonnet, and refer to [BGN19] for more sophisticated schemes. See [MU24b, §2.2] for comments on and illustrations of convergence of the used FEM.

Technically, for the 4th order problem (5) we use a mixed formulation as two 2nd order problems, first analyzed in [Rus05] (in a more complicated scheme); see [SGJW22] for a convergence analysis in the frame of the biharmonic equation. Additionally to the PDE $\eta(u)\partial_t u = G(u, \Lambda)$ and the constraints $q(u) = 0$, the continuation needs phase conditions (PCs), for which we introduce additional Lagrange multipliers s_x, s_y, s_z and s_{rx} pertaining to translations in x, y and z, respectively, and rotations around the x–axis. The y–and z–translation PCs are always on, the x–translations is on for pearling and coiling, the x–rotation in on for the wrinkling, and x–translation *and* rotation are on for the buckling. In all continuations, the associated Lagrange multipliers stay 10^{-6}. For the discrete systems, an effect of all the constraints (also of $q(u) = 0$) is that the linear systems (to be solved in Newton loops and for eigenvalue computations) are bordered, with border widths up to six rows/columns, and we usually use bordered elimination [Uec21, §4.5.1] for their solution.

Mesh handling. The initial cylinder in discretized by a standard mesh from `pde2path`, mapped via a local map on the cylinder. The number of nodes in x and φ direction is chosen to minimize the mesh–quality quotient

$$q = \max_{T \in \mathcal{T}} \frac{e_M(e_1 + e_2 + e_3)}{2|T|}, \tag{66}$$

with e_j the edge lengths, e_M the maximal edge length, and $|T|$ the triangle areas. The triangulation is oriented inwards, matching with the above convention. On the bifurcating branches triangles distort, due to the change of X. We use mesh adaptation by refinement and coarsening of X and `tri` based on (66) and triangle areas. Namely, we refine if the area is above a threshold, typically 1.3 times the size of the original cylinder triangles. For the conservation of the periodic boundary, we enforce the same refinement at "opposite" boundary triangles. For the coarsening (66) is the control parameter, activated if $q > 8$. We select triangles smaller than a threshold A_t, typically $A_t = \max_{T \in \mathcal{T}} |T|/3$ and collapse acute triangles along the shortest edge, while obtuse triangles are handled with edge flipping.

Periodicity in x. During the continuation of bifurcating branches, it is not necessary that the boundary of X stays in a plane. However, for mesh refinement along the branch the legacy `box2per` setting looks for periodic boundary nodes in planes. For that reason we only allow an (y, z) displacement at the boundary, by setting $N_x = 0$.

Extracting the amplitude. For the comparison between the numerics and the AE predictions, we evaluate the deviation at each mesh point. In each continuation step we obtain $X + uN$ as the new solution, but multiple steps result in tangential movement of mesh points relative to the cylinder. Therefore we project each mesh point back onto the cylinder orthogonally to $Cp = \left(p_1, \frac{p_2}{\|(p_2, p_3)\|}, \frac{p_3}{\|(p_2, p_3)\|}\right)^T$. From this projection, we can measure the normal deviation from the cylinder and compare it with the amplitude approximation.

On the volume in the numerics. To compute the volume of (not necessarily straight) cylinders $\mathcal{C}$ we split them into two domains Ω_1 and Ω_2, see Fig.13, where $\Omega_2 = \Omega_{2,a} \cup \Omega_{2,b}$ consists of two equal cones, from $(x, y, z) = (0, 0, 0)$ to the (in general not circular) left and right disk at $x = \pm L/2$. The idea is to compute $V = \text{vol}(\Omega_1) + 2\text{vol}(\Omega_{2a})$ by the divergence theorem $\text{vol}(\Omega) = \frac{1}{3}\int_\Omega \text{div}(x)\,\mathrm{d}x = \frac{1}{3}\int_{\partial\Omega}\langle x, N\rangle\,\mathrm{d}S$. In the splitting $\mathcal{C} = \Omega_1 \cup \Omega_2$, we have $\langle x, N\rangle = 0$ along the inner "conical" boundaries $\partial\Omega_1 \cap \partial\Omega_2$, such that $\text{vol}(\Omega_1) = \frac{1}{3}\int_X \langle (x, y, z), N\rangle\,\mathrm{d}S$, and $\text{vol}(\Omega_{2a}) = \frac{1}{3}\int_{X_{\text{left}}} \langle (-L/2, 0, 0)^T, (-1, 0, 0)^T\rangle\,\mathrm{d}(y, z) = \frac{L}{2}|X_{\text{left}}|$, and for the latter we can apply Gauss' theorem again to obtain

$$\text{vol}(\Omega_{2a}) = \frac{L}{6}\frac{1}{2}\int_{\partial X_{\text{left}}} \langle (y, z), (\nu_1, \nu_2)\rangle\,\mathrm{d}s = \frac{L}{12}\int_{\partial X_{\text{left}}} \langle (X_2, X_3), (N_2, N_3)/\|(N_2, N_3)\|\rangle\,\mathrm{d}s. \qquad (67)$$

Thus, altogether,

$$\text{vol}(\mathcal{C}) = \frac{1}{3}\int_X \langle (x, y, z), N\rangle\,\mathrm{d}S + \frac{L}{6}\int_{\partial X_{\text{left}}} \langle (X_2, X_3), (N_2, N_3)/\|(N_2, N_3)\|\rangle\,\mathrm{d}s. \qquad (68)$$
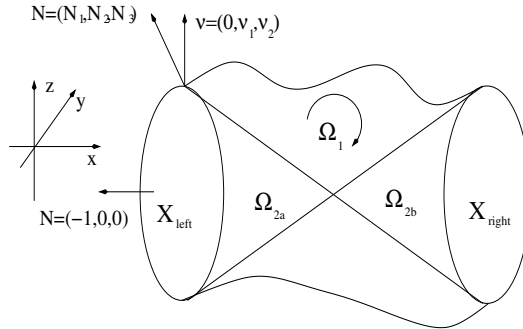

Figure 13: Sketch for volume computation.

In the numerics we also need the derivative of $V(\mathcal{C} + uN)$ wrt u. For $\Omega = \Omega_0 + uN$ and $\text{vol}(\Omega) = \frac{1}{3}\int_{\partial\Omega}\langle X, N\rangle\,\mathrm{d}S$ we have $\partial_u\text{vol}(\Omega)v = \int_\Omega v\,\mathrm{d}S$, which can be used for $\partial_u\text{vol}(\Omega_1)$, and for $\partial_u\text{vol}(\Omega_{2a})$ we proceed as follows. We choose a positive oriented arc length parametrization $\gamma : [0, 2\pi) \to \partial X_{\text{left}}$. Then the (unit) tangent and (unit) normal vectors are $T(s) = \left(\gamma_1'(s), \gamma_2'(s)\right)^T$ and $\nu(s) = \left(-\gamma_2'(s), \gamma_1'(s)\right)^T$. For a perturbation u we consider $\tilde{\gamma}(s) = \gamma(s) + \delta u(s)\nu(s) = \begin{pmatrix} \gamma_1(s) - \delta u(s)\gamma_2'(s) \\ \gamma_2(s) + \delta u(s)\gamma_1'(s) \end{pmatrix}$, with unit normal

vector $\tilde{\nu} = \begin{pmatrix} -\tilde{\gamma}_2'(s) \\ \tilde{\gamma}_1'(s) \end{pmatrix} / \|\tilde{\gamma}'(s)\|$. Then

$$
\begin{aligned}
\frac{\mathrm{d}}{\mathrm{d}\delta}\Big|_{\delta=0} \int_0^{2\pi} \langle \tilde{\gamma}(s), \tilde{\nu}(s)\rangle \|\tilde{\gamma}'(s)\| \, \mathrm{d}s &= \frac{\mathrm{d}}{\mathrm{d}\delta}\Big|_{\delta=0} \int_0^{2\pi} \tilde{\gamma}_2(s)\tilde{\gamma}_1'(s) - \tilde{\gamma}_1(s)\tilde{\gamma}_2'(s) \, \mathrm{d}s \\
&= \int_0^{2\pi} \frac{\mathrm{d}}{\mathrm{d}\delta}\Big|_{\delta=0} \Big[\big(\gamma_2(s) + \delta u(s)\gamma_1'(s)\big)\big(\gamma_1'(s) - \delta\big(u(s)\gamma_2'(s)\big)'\big) \\
&\qquad - \big(\gamma_1(s) - \delta u(s)\gamma_2'(s)\big)\big(\gamma_2'(s) + \delta\big(u(s)\gamma_1'(s)\big)'\big) \Big] \, \mathrm{d}s \\
&= \int_0^{2\pi} u(s)\gamma_1'(s)^2 - \gamma_2(s)(u(s)\gamma_2'(s))' + u(s)\gamma_2'(s)^2 - \gamma_1(s)(u(s)\gamma_1'(s))' \, \mathrm{d}s = 2\int_0^{2\pi} u(s)\,\mathrm{d}s,
\end{aligned}
$$

which can be easily implemented using the (1D) mass matrix of the discretization of $\partial X_{\mathrm{left}}$.

Numerical flows. We give a brief description of our ad hoc method for numerical flows (aka direct numerical simulation DNS) for (5), and refer to [BMN05, BGN08, BGN20, BGN21] and the references therein for more sophisticated and provably stable FEM schemes for geometric flows, including the Helfrich flow (5) and extensions, and in particular also dealing with tangential motion of mesh points. Here we only consider normal displacements, and approximate the normal velocity as

$$
V_t = \langle \partial_t X, N\rangle \approx \left\langle \frac{1}{h} M_n(X_{n+1} - X_n), N_n \right\rangle = \frac{1}{h} \langle M_n(X_n + u_{n+1}N_n - X_n), N_n \rangle = \frac{1}{h} M_n u_{n+1},
$$

where h is the current stepsize, n the time stepping index, and M_n the mass matrix. Setting $U_n = (u_n, \Lambda_n)$, the PDE $V_t = G(X(t), \Lambda(t))$, together with the (volume and area) constraints $q(u_{n+1}) = 0$ (translational and rotational phase conditions play no role in the DNS), yields the nonlinear system

$$
\mathcal{G}(U_{n+1}) := \begin{pmatrix} \frac{1}{h} M_n u_{n+1} + G(U_{n+1}) \\ q(u_{n+1}) \end{pmatrix} \overset{!}{=} \begin{pmatrix} 0 \\ 0 \end{pmatrix} \in \mathcal{H} \times \mathbb{R}^{n_q} \tag{69}
$$

for U_{n+1}, where $\mathcal{H}$ stands for the FEM space used. Given h and X_n, we solve (69) for U_{n+1}, up to a given tolerance `tol`, usually `tol` $= 10^{-6}$ in the sup–norm, via Newton loops. For simplicity we do not apply an extrapolation step, i.e., the initial guesses for the Newton loops are $u_{n+1}^{(0)} = 0$ (because X_n has already been updated) and $\Lambda_{n+1}^{(0)} = \Lambda_n$. Note that there are no initial conditions for Λ (only for X_0, which corresponds to $u_0 = 0$), and we use $\Lambda_1^{(0)} = \Lambda_0$, the values of Λ at the steady state which we perturb. For the Newton loops we essentially have all tools (in particular Jacobians) available from the continuation setup. This also suggest some time stepping control (decrease h if many Newton iterations required or no convergence, increase h if fast convergence).

Additionally we remark that Newton loops for (69) often fail to converge near straight cylinders (or more generally CMC surfaces), where $\partial_u q_1$ and $\partial_u q_2$ become linearly dependent ($\mathcal{D}$ from (19) becomes singular), but this is not a major concern for us as we are more interested in the flow towards nontrivial steady states. See, e.g., [BGN08, Scheme (2.8)] for dealing with the constraints when approaching CMC surfaces, which essentially consists in setting $\lambda_{1,n+1} = \lambda_{1,n}$ and only solving for $\lambda_{2,n+1}$ with $q(u_{n+1}) = q_2(u_{n+1})$. Moreover, the DNS in §5 are all uncritical wrt to mesh quality. However, for stronger initial perturbations we expect that allowing and controlling tangential motion of mesh points (or other ways of mesh–adaptation) will be crucial, see also, e.g., the numerical flows for closed vesicles in [MU24a].

References

[Aub82]   Th. Aubin. *Nonlinear analysis on manifolds, Monge-Ampère equations.* Springer, 1982.

[BDGP23]   E. Bänsch, K. Deckelnick, H. Garcke, and P. Pozzi. *Interfaces: modeling, analysis, numerics*, volume 51 of *Oberwolfach Seminars.* Birkhäuser/Springer, Cham, 2023].

[BGN08]   J. Barrett, H. Garcke, and R. Nürnberg. Parametric approximation of Willmore flow and related geometric evolution equations. *SIAM J. Sci. Comput.*, 31(1):225–253, 2008.

[BGN19]   J. Barrett, H. Garcke, and R. Nürnberg. Finite element methods for fourth order axisymmetric geometric evolution equations. *J. Comput. Phys.*, 376:733–766, 2019.

[BGN20]   J. Barrett, H. Garcke, and R. Nürnberg. Parametric finite element approximations of curvature-driven interface evolutions. In *Geometric partial differential equations. Part I*, volume 21 of *Handb. Numer. Anal.*, pages 275–423. Elsevier, Amsterdam, 2020.

[BGN21]   J. Barrett, H. Garcke, and R. Nürnberg. Stable approximations for axisymmetric Willmore flow for closed and open surfaces. *ESAIM Math. Model. Numer. Anal.*, 55(3):833–885, 2021.

[BHAVMC17]   E. Beltran-Heredia, V. Almendro-Vedia, F. Monroy, and F. Cao. Modeling the mechanics of cell division: Influence of spontaneous membrane curvature, surface tension, and osmotic pressure. *Frontiers in Physiology*, 8(312):1–19, 2017.

[BK07]   J. Burke and E. Knobloch. Homoclinic snaking: Structure and stability. *Chaos*, 17(3):037102, 2007.

[BKL+09]   M. Beck, J. Knobloch, D.J.B. Lloyd, B. Sandstede, and T. Wagenknecht. Snakes, ladders, and isolas of localized patterns. *SIAM J. Math. Anal.*, 41(3):936–972, 2009.

[BMN05]   E. Bänsch, P. Morin, and R. Nochetto. A finite element method for surface diffusion: the parametric case. *J. Comput. Phys.*, 203(1):321–343, 2005.

[BZM94]   R. Bar-Ziv and E. Moses. Instability and 'pearling' states produced in tubular membranes by competition of curvature and tension. *PRL*, 73:1392–1395, 1994.

[Can70]   P. Canham. The minimum energy of bending as a possible explanation of the biconcave shape of the human red blood cell. *Journal of Theoretical Biology*, 26:61–81, 1970.

[CL00]   P. Chossat and R. Lauterbach. *Methods in equivariant bifurcations and dynamical systems.* World Scientific Publishing Co., Inc., River Edge, NJ, 2000.

[CR98]   S. Chaieb and S. Rica. Spontaneous curvature-induced pearling instability. *PRE*, 58:7733, 1998.

[FTGB+99]   V. Frette, I. Tsafrir, M. Guedeau-Boudeville, L. Jullien, D. Kandel, and J. Stavans. Coiling of cylindrical membrane stacks with anchored polymers. *PRL*, 83(12):2465–2468, 1999.

[FVKG22]   B. Foster, N. Verschueren, E. Knobloch, and L. Gordillo. Pressure-driven wrinkling of soft inner-lined tubes. *New J. Phys.*, 24:013026, 2022.

[Gar13]   H. Garcke. Curvature driven interface evolution. *Jahresber. Dtsch. Math.-Ver.*, 115(2):63–100, 2013.

[GNPS96]   R.E. Goldstein, P. Nelson, T. Powers, and U. Seifert. Front progagation in the pearling instability of tubular vesicles. *J.Phys.II*, 6:767–796, 1996.

[GS02]   M. Golubitsky and I. Stewart. *The symmetry perspective.* Birkhäuser, Basel, 2002.

[HEJ+14]   D. Heinrich, M. Ecke, M. Jasnin, U. Ecke, and G. Gerisch. Reversible membrane pearling in live cells upon destruction of the actin cortex. *Biophysical Journal*, 106:1079–1091, 2014.

[Hel73]   W. Helfrich. Elastic properties of lipid bilayers: Theory and possible experiments. *Zeitschrift für Naturforschung*, 28:693, 1973.

[Hen81]   D. Henry. *Geometric Theory of Semilinear Parabolic Equations*. Springer Lecture Notes in Mathematics, Vol. 840, 1981.

[Hil20]   B. Hilder. Modulating traveling fronts for the swift-hohenberg equation in the case of an additional conservation law. *J. Differential Equations*, 269(5):4353–4380, 2020.

[HK09]   S. M. Houghton and E. Knobloch. Homoclinic snaking in bounded domains. *Phys. Rev. E*, 80:026210, 2009.

[Hoy06]   R.B. Hoyle. *Pattern formation*. Cambridge University Press., 2006.

[Jac24]   A. Jacobson. gptoolbox, `https://github.com/alecjacobson/gptoolbox`, 2024.

[JSL93]   F. Jülicher, U. Seifert, and R. Lipowsky. Phasediagrams and shape transformations of toroidal vesicles. *J.Phys.II*, 3:1681–1705, 1993.

[Kno15]   E. Knobloch. Spatial localization in dissipative systems. *Annu.Rev.Condens.Matter Phys.*, 6:325–359, 2015.

[Lie15]   St. Liebscher. *Bifurcation without parameters*, volume 2117 of *Lecture Notes in Mathematics*. Springer, Cham, 2015.

[LM72]   J.-L. Lions and E. Magenes. *Non-homogeneous boundary value problems and applications, Vol. I–III*. Springer, 1972.

[LS16]   J. LeCrone and G. Simonett. On the flow of non-axisymmetric perturbations of cylinders via surface diffusion. *J. Differential Equations*, 260(6):5510–5531, 2016.

[Lun95]   A. Lunardi. *Analytic semigroups and optimal regularity in parabolic problems*. Birkhäuser Verlag, Basel, 1995.

[MRS13]   M. Meyries, Jens D. M. Rademacher, and E. Siero. Quasi-linear parabolic reaction-diffusion systems: A user's guide to well-posedness, spectra, and stability of travelling waves. *SIAM J. Appl. Dyn. Syst.*, 13:249–275, 2013.

[MU24a]   A. Meiners and H. Uecker. Differential geometric bifurcation problems in `pde2path` – algorithms and tutorial examples, 2024. Available at [pde25].

[MU24b]   A. Meiners and H. Uecker. Numerical continuation and bifurcation for differential geometric PDEs. *Numerical Mathematics – Theory Mehods Applications*, 2024.

[NSS15]   V. Narsimhan, A. P. Spann, and E. S. G. Shaqfeh. Pearling, wrinkling, and buckling of vesicles in elongational flows. *J. Fluid Mech.*, 777:1–26, 2015.

[NY12]   Takeyuki Nagasawa and Taekyung Yi. Local existence and uniqueness for the n-dimensional Helfrich flow as a projected gradient flow. *Hokkaido Math. J.*, 41(2):209–226, 2012.

[pde25]   pde2path. `https://pde2path.uol.de/`, 2025.

[Pet83]   Mark A. Peterson. An instability of the red blood cell shape. *J. of Applied Physics*, 57:1739–1742, 1983.

[PQAEM09] G. Paredes-Quijada, H. Aranda-Espinoza, and A. Maldonado. Shapes and coiling of mixed phospholipid vesicles. *Lipids*, 44:283–289, 2009.

[RSS24]   F. Rupp, C. Scharrer, and M. Schlierf. Gradient flow dynamics for cell membranes in the Canham-Helfrich model, `https://arxiv.org/pdf/2408.07493`, 2024.

[Rus05]   R. E. Rusu. An algorithm for the elastic flow of surfaces. *Interfaces Free Bound.*, 7(3):229–239, 2005.

[SBL90]   U. Seifert, K. Berndl, and R. Lipowsky. Shape transformations of vesicles: Phase diagram. *PRA*, 44:1182–1202, 1990.

[Sch24]   R. Schnaubelt. Lecture Notes Evolution Equations, `https://www.math.kit.edu/iana3/~schnaubelt/media/evgl-skript.pdf`, 2024.

[Sei97]   U. Seifert. Configurations of fluid membranes and vesicles. *Advances in Physics*, 46(1):13–137, 1997.

[SGJW22]   O. Stein, E. Grinspun, A. Jacobson, and M. Wardetzky. A mixed finite element method with piecewise linear elements for the biharmonic equation on surfaces, `http://arxiv.org/pdf/1911.08029`, 2022.

[Sim95]   G. Simonett. Center manifolds for quasilinear reaction-diffusion systems. *Differential and Integral Equations*, 8(4):753 – 796, 1995.

[SL95]   U. Seifert and R. Lipowsky. Morphology of Vesicles. In R.Lipowsky and E. Sackmann, editors, *Handbook of Biological Physics*, volume 1, pages 403–463. Elsevier, 1995.

[Sta01]   J. Stavans. Instabilities of membranes with anchored polymers. *Physica A*, 306:368–375, 2001.

[SU17]   G. Schneider and H. Uecker. *Nonlinear PDE – a dynamical systems approach*, volume 182 of *Graduate Studies Mathematics*. AMS, Providence, RI, 2017.

[SZ89]   S. Svetina and B. Zeks. Membrane bending energy and shape determination of phospholipid vesicles and red blood cells. *Eur.Biophys J,*, 17(2):101–111, 1989.

[Tap16]   K. Tapp. *Differential geometry of curves and surfaces*. Springer, [Cham], 2016.

[TGBKS01]   I. Tsafrir, M. Guedeau-Boudeville, D. Kandel, and J. Stavans. Coiling instability of multilamellar tubes with anchored polymers. *PRE*, 63:031603, 2001.

[Tri78]   H. Triebel. *Interpolation theory, function spaces, differential operators*. VEB Deutscher Verlag der Wissenschaften, Berlin, 1978.

[TSA+01]   I. Tsafrir, D. Sagi, T. Arzi, M. Guedeau-Boudeville, V. Frette, D. Kandel, and J. Stavans. Pearling instabilities of membrane tubes with anchored polymers. *PRL*, 86(6):1138–1141, 2001.

[Uec21]   H. Uecker. *Numerical continuation and bifurcation in Nonlinear PDEs*. SIAM, Philadelphia, PA, 2021.

[UY17]   Masaaki Umehara and Kotaro Yamada. *Differential geometry of curves and surfaces*. World Scientific, 2017. Translated from the second (2015) Japanese edition by W.Rossman.

[ZcH89]   Ou-Yang Zhong-can and W. Helfrich. Bending energy of vesicle membranes: General expressions for the first, second, and third variation of the shape energy and applications to spheres and cylinders. *Physical review A*, 39 10:5280–5288, 1989.

[ZS16]   D. Zimmermann and G. Schneider. The Turing instability in case of an additional conservation law – Dynamics near the Eckhaus boundary and open questions. In *Proceedings of Pattern of Dynamics*, pages 28–43. Springer, 2016.